

Big Bang Nucleosynthesis as a Probe of New Physics

MAXIM POSPELOV*

Perimeter Institute for Theoretical Physics, Waterloo, ON, N2L 2Y5, Canada
Department of Physics and Astronomy, University of Victoria, Victoria, BC, V8P 1A1,
Canada

JOSEF PRADLER[†]

Perimeter Institute for Theoretical Physics, Waterloo, ON, N2L 2Y5, Canada

Key Words Big bang nucleosynthesis, early Universe, abundances of light elements, extensions of the Standard Model, dark matter

Abstract Big bang nucleosynthesis (BBN), an epoch of primordial nuclear transformations in the expanding Universe, has left an observable imprint in the abundances of light elements. Precision observations of such abundances, combined with high-accuracy predictions, provide a nontrivial test of the hot big bang and probe non-standard cosmological and particle physics scenarios. We give an overview of BBN sensitivity to different classes of new physics: new particle or field degrees of freedom, time-varying couplings, decaying or annihilating massive particles leading to non-thermal processes, and catalysis of BBN by charged relics.

CONTENTS

INTRODUCTION	2
<i>Universe at redshift of a billion: basic assumptions and main stages of BBN</i>	4
NEW PHYSICS AFFECTING THE TIMING OF MAIN BBN EVENTS	12
<i>BBN with new degrees of freedom</i>	12
<i>BBN with sliding couplings and mass scales.</i>	14
NON-EQUILIBRIUM BBN	15
<i>BBN with electromagnetic and hadronic energy injection</i>	16
<i>Energy injection by WIMPs</i>	23
CATALYZED BBN	25
<i>Catalysis by stable charged particles.</i>	26
<i>Catalysis by strongly interacting relics</i>	30
CONCLUSIONS	31

1 INTRODUCTION

The model of the hot expanding Universe, once the subject of fierce scientific and philosophical debate, is now a well-established reality. Explosive progress in the field of cosmology over the past decade allowed for something that may well have been totally unanticipated in the previous decades: the high-precision determination of several cosmological parameters. This recent progress primarily clarifies the state of the Universe at redshifts $z \lesssim$ few and exposes the relevant physics of the Universe traced back to the epoch of the decoupling of the cosmic microwave background (CMB) at $z \lesssim 10^3$. At the same time, these recent advances also allow one to check for the consistency with one the building blocks of modern cosmology: big bang nucleosynthesis (BBN). The agreement, or rather the lack of qualitative disagreement between cosmology in the $z = 0 - 10^3$ interval and BBN at $z \sim 10^9$, is very important, as it leads to the conclusion that the very early Universe was governed by the same physical laws of nature as the current Universe and that it contained very similar if not identical particle content. Remarkably, that the transformations and the synthesis of light elements in the expanding Universe occur with the active participation of all the interactions known to date: strong, weak, electromagnetic, and gravitational. It is well known that even a mild modification of the standard conditions in the early Universe, at the time of BBN or in the subsequent evolution, may lead to observable deviations in primordial abundances. Thus, employing the precise determinations of the primordial abundances allows one to set limits or constrain various scenarios with deviations from General Relativity or from particle physics of the Standard Model (SM).

*pospelov@uvic.ca

†jpradler@perimeterinstitute.ca

Primordial nucleosynthesis is not the earliest cosmological epoch. It must have been preceded by an era in which a mechanism capable of producing the observed baryon-antibaryon asymmetry of the Universe (baryogenesis) was operative. Moreover, a period of generation of nearly scale-invariant cosmological perturbations—for which the leading candidate is inflation—had set the initial conditions from which the large-scale structure of the Universe evolved. Neither the cosmological timing nor the main “players” in inflation or baryogenesis—such as the inflaton, the right-handed neutrino, and so on—are known with certainty. Although many successful models of this earliest epoch(s) exist, it is extremely difficult to directly test the associated physics in the laboratory. Thus, a multitude of baryogenesis- and inflationary scenarios may be viable. In contrast, BBN relies on very well-studied pieces of physics, such as spectra and reactions of light elements and their weak decays. It involves almost no free parameters and occurs in a well-understood sequence of events in the early Universe. The consistency of BBN predictions with observations imposes an important calibration point on all new models of particle physics that require them to achieve some degree of “normalcy” before $t = 1$ s. This requirement places powerful constraints on many extensions of the SM.

The purpose of this review is to reveal different physical mechanisms by which new physics can affect BBN and its light element abundance predictions, which have been extensively discussed in the literature for as long as the BBN theory has existed. In fact, one of the first papers on the subject by Alpher, Follin and Herman [1] points out that the nature of the neutrino species (Dirac versus Majorana) affects the neutron-to-proton freeze-out ratio, n/p , and thereby the primordial helium abundance. Since then, a great deal of research dedicated to non-standard BBN scenarios has been performed, and a number of different ways in which new physics can change the outcome of BBN have been identified. Here, we present a non-technical review of many aspects related to these interesting possibilities.

The developments of the past decade also confirmed the conclusion that the SM is not the ultimate theory. Important pieces of the puzzle come from cosmological observations suggesting that the energy balance of the modern Universe is dominated by dark energy and dark matter. Is it possible that physics related to these mysterious substances interfered with the sequence of events that ultimately led to the fusion of the primordial elements? Although there is no compelling evidence that this occurred, some new physics models related to particle dark matter may reduce the tension between data and the standard BBN theory (SBBN) prediction for the lithium isotopes. Even though the resolution of this tension may be related to astrophysics, it is nevertheless intriguing to entertain the possibility that the relics of the early Universe may hint at deviations from the SM. Future developments in astrophysics, cosmology, and particle physics may help to clarify this question.

1.1 Universe at redshift of a billion: basic assumptions and main stages of BBN

The primary activity of BBN took place in the era associated with photon temperatures between $T \simeq \text{few MeV}$ and $T \simeq 10 \text{ keV}$, in the cosmic time window $t \simeq (0.1 \div 10^4) \text{ s}$, and may be considered as a transition from a neutron-proton statistical equilibrium with no other nuclear species to a Universe with a significant presence of helium. BBN produced the bulk of ${}^4\text{He}$ and D as well as good fractions of ${}^3\text{He}$ and ${}^7\text{Li}$ observed in the current Universe. All the other elements are believed to be produced either by stars or by cosmic rays.

We begin by specifying the main assumptions on which SBBN theory rests:

1. It is assumed that the Universe is spatially homogeneous and isotropic and that its energy density is completely dominated by radiation so that physical distances scale as $a(t) \propto t^{1/2}$. It is also assumed that the space-time geometry is flat with zero spatial curvature. The theory of general relativity relates the expansion rate with the time elapsed since the big bang and with the energy density of the ambient cosmological fluid ρ :

$$H \equiv \frac{\dot{a}}{a} = \sqrt{8\pi G_N \rho/3} \simeq \frac{1}{2t}, \quad (1)$$

where the energy density of the radiation-dominated Universe scales as $\rho \sim a^{-4} \sim T^4$; G_N denotes Newton's constant $G_N = (8\pi M_{\text{Pl}}^2)^{-1}$ where $M_{\text{Pl}} \simeq 2.43 \times 10^{18} \text{ GeV}$ is the reduced Planck mass. It is also assumed that the dark matter and dark energy components of the Universe are “well-behaved”, that is, that their contribution to the energy density at the time of BBN is negligible.

2. It is assumed that the initial temperature of the radiation-dominated epoch of the Universe was well above the neutron-proton mass difference $\Delta m_{np} = 1.293 \text{ MeV}$, so that the initial conditions for the nuclear reaction framework are well specified:

$$(n_n \simeq n_p)|_{T \gg \Delta m_{np}} = \frac{1}{2} n_b. \quad (2)$$

The energy-momentum distribution of neutrons and protons is very close to being thermal. Moreover, a near-perfect spatial homogeneity for the distributions of neutrons and protons is assumed.

3. It is assumed that the particle content and their interactions are given by that of the SM and that by the time of BBN the baryon asymmetry was already present. The energy density is completely dominated by photons and the three species of SM neutrinos (as well as electrons and positrons before their annihilation), whereas neutrons and protons carry only a negligible fraction of the total energy density. The standard field content implies that there was an “uneventful” cosmological period between the time of BBN and the epoch of hydrogen recombination with electrons which implies that the baryon-to-entropy density ratio measured at the period of

CMB-“formation” directly translates into the one at BBN:

$$\frac{n_b}{s}(t_{\text{BBN}}) = \frac{n_b}{s}(t_{\text{CMB}}). \quad (3)$$

Indeed, the measurements of the Wilkinson Microwave Anisotropy Probe (WMAP) satellite have allowed us to pinpoint the baryon density for a standard Λ CDM cosmology, that is a flat Universe filled with baryons, cold dark matter, neutrinos and a cosmological constant, to an accuracy of better than 3% [2]. Expressed in terms of the baryon-to-photon ratio,

$$\eta_b(t_{\text{CMB}}) = \frac{n_b}{n_\gamma}(t_{\text{CMB}}) = (6.23 \pm 0.17) \times 10^{-10}, \quad (4)$$

this number provides a measure of the nucleon content of the Universe at BBN.

4. Finally, it is assumed that the properties of particles and nuclei (masses, couplings, scattering cross sections and lifetimes) are identical between their current values and their values at t_{BBN} . This condition, in fact, follows from the assumption of a minimal field content, as hypothetical changing couplings and masses would necessitate new ultra-soft scalar fields.

In many theories with non-standard cosmological or particle physics content, some of these assumptions can be violated. For example, “late decays”, that is, decays of metastable heavy particles during or after BBN can lead to energy injection into the primordial plasma and thus to temporary but strong departures from thermal equilibrium for some species. The presence of the new relativistic degrees of freedom may affect the total energy density of the Universe, and, by modifying the Hubble expansion rate, may change the outcome of nuclear reactions. Before we consider such modifications in more detail, we remind the reader of the main components of the SBBN and briefly review its current observational status.

SBBN theory, including the hits and misses of the original papers [3, 4, 5], is now well understood and described in detail in many text-books and reviews [6, 7, 8, 9, 10]. SBBN comprises the set of first-order differential Boltzmann equations on the abundances of the different species,

$$\frac{dY_i}{dt} = -H(T)T \frac{dY_i}{dT} = \sum (\Gamma_{ij}Y_j + \Gamma_{ikl}Y_kY_l + \dots), \quad (5)$$

where $Y_i = n_i/n_b$ are the time t (or temperature T)-dependent ratios between the number density n_i and the baryon number density n_b of light elements $i = p, n, \text{D}, ^4\text{He}$, and so on. The $\Gamma_{ij\dots}$ represent generalized rates for element interconversion and decay that can be determined in experiments and/or inferred from theoretical calculations. $H(T)$ is the temperature-dependent Hubble expansion rate from Eq. (1).

The full form of the (non-integrated) Boltzmann equations should be given in terms of particle distribution functions over energy and momenta. However, in practice, the system of equations (5), which assumes thermal distributions for nuclei, provides an excellent

approximation because the frequent interactions with the numerous γ s and e^\pm s in the plasma keep the light elements tightly coupled to the radiation field. The dependence of $H(T)$ on the temperature of the primordial plasma can be further specified:

$$H(T) = T^2 \left(\frac{8\pi^3 g_* G_N}{90} \right)^{1/2}, \quad \text{where } g_* = g_{\text{boson}} + \frac{7}{8} g_{\text{fermion}}, \quad (6)$$

where the g s denote the excited relativistic degrees of freedom. This expression needs to be interpolated across the electron-positron annihilation epoch, in which the photon bath is heated with respect to the neutrino reservoir. The neutrinos maintain a quasi-thermal spectrum with temperature

$$T_\nu \simeq (4/11)^{1/3} T, \quad (7)$$

in the approximation of full neutrino decoupling at the time of electron-positron annihilation [with small calculable corrections [11]]. Following e^\pm annihilation, the Hubble rate is given by $H(T) \simeq T_9^2 / (2 \times 178 \text{ s})$, where T_9 denotes the photon temperature T in units of 10^9 K .

A number of well-developed integration codes, pioneered by Wagoner et al. [12], allow one to solve the BBN system of equations numerically and to obtain the freeze-out values of the light elements. Also, good semi-analytic results can be obtained, see *e.g.* Ref. [13]. The code that we use for this review is based on that of Ref. [14]. Here we incorporate some significant improvements and updates; physical constants, isotope masses, and conversion factors are determined from the evaluations [15, 16]. For all important SBBN reactions (*i.e.* up to $A=7$) we employ the results of [17] with the exceptions of the $n(p, \gamma)\text{D}$ and ${}^3\text{He}(\alpha, \gamma){}^7\text{Be}$ reactions for which we follow [18] and [19], respectively. To arrive at an accurate prediction of ${}^4\text{He}$, we numerically integrate all weak rates at each time step for which zero temperature radiative corrections as well as relativistic Coulomb corrections (when applicable) are taken into account [20, 21]. Finally, as assessed in [20], we apply a slight upward-shift of 0.72% of the resulting ${}^4\text{He}$ abundance to account for more subtle, subleading corrections to the BBN reaction network. We then find very good agreement between our light element-abundance predictions and those presented in [22] at the WMAP value (4) and with a neutron lifetime of $\tau_n = 885.7 \text{ s}$.

Figure 1 shows the output of the SBBN reaction network. The evolution of all the main isotopes with $A \leq 7$ is plotted as a function of time and temperature. Beginning from the earliest times, the following sequence of events occurs: (a) the chemical decoupling of neutrinos from the thermal bath, (b) the annihilation of electrons and positrons, (c) the freeze-out of neutrons and protons, (d) an “intermission” between the n/p freeze-out and the deuteron ignition at the end of the “bottleneck,” (e) helium synthesis at $T_9 \simeq 0.85$ (70 keV), and finally (f) a follow-up stage in which the main nuclear reactions gradually drop out of equilibrium and the abundances of all light elements freeze out. The freeze-out abundances are given by the horizontal lines on the right-hand side of the graph. Although some neutrons are still generated by residual deuterium (D) fusion below $T_9 \sim 0.1$ (10 keV), they are too few in number to cause any further change in the elemental abundances.

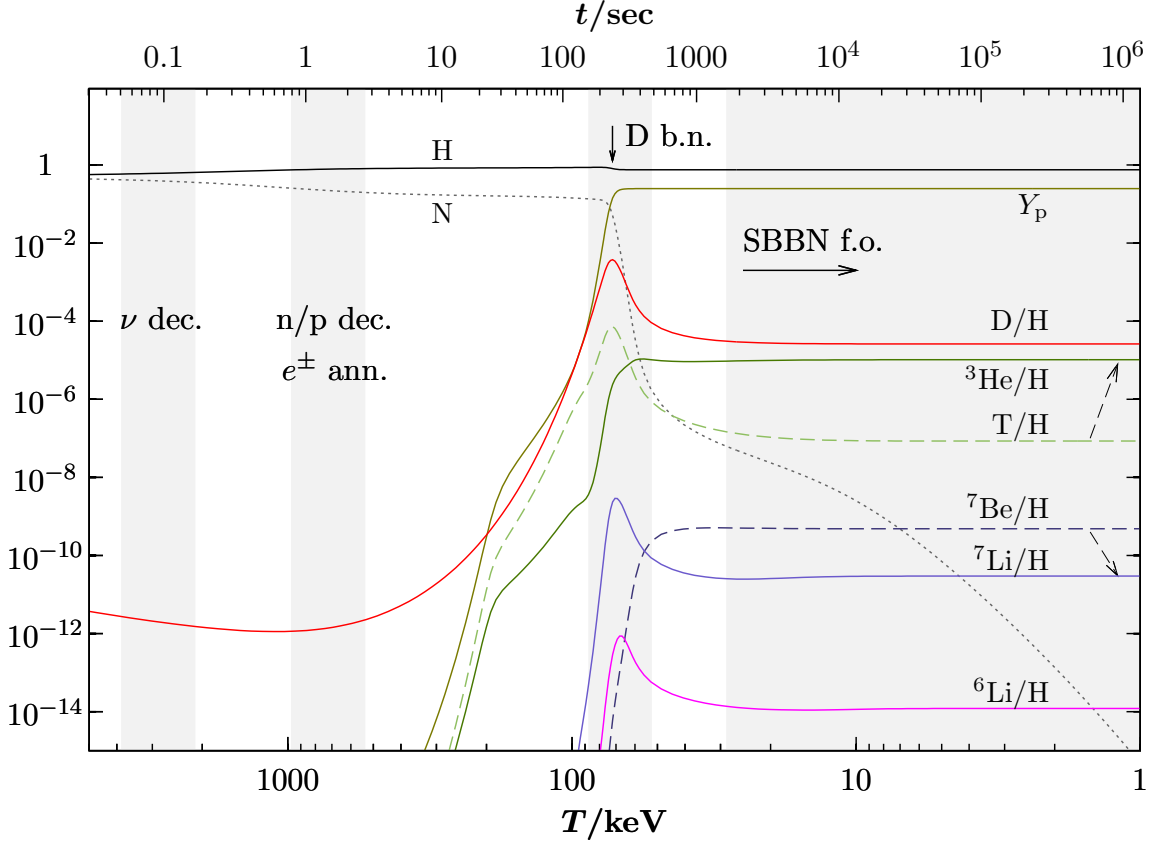


Figure 1: Time and temperature evolution of all standard big bang nucleosynthesis (SBBN)-relevant nuclear abundances. The vertical arrow indicates the moment at $T_9 \simeq 0.85$ at which most of the helium nuclei are synthesized. The gray vertical bands indicate main BBN stages. From left to right: neutrino decoupling, electron-positron annihilation and n/p freeze-out, D bottleneck, and freeze-out of all nuclear reactions. Protons (H) and neutrons (N) are given relative to n_b whereas Y_p denotes the ${}^4\text{He}$ mass fraction.

Below we discuss the fusion of the light elements and compare their SBBN predictions with observations.

1.1.1 $\mathcal{O}(0.1)$ ABUNDANCES: ${}^4\text{He}$. The beauty of the SBBN prediction for ${}^4\text{He}$ lies in its simplicity. Only a few factors that determine it. The rates for weak scattering processes that inter-convert $n \leftrightarrow p$ at high plasma temperatures scale as $G_F^2 T^5$, where G_F is the Fermi constant. As the Universe cools, these rates drop below the T^2 -proportional Hubble rate $H(T)$ Eq. (6). The neutron-to-proton transitions slow down, and the ratio of their respective number densities cannot follow its chemical-equilibrium exponential dependence, $n/p|_{\text{eq}} \simeq \exp(-\Delta m_{np}/T)$. Around $T \simeq 0.7 \text{ MeV}$ this dependence freezes out to $n/p \simeq 1/6$ but continues to decrease slowly due to residual scattering and β -decays of neutrons. The formation of D during this intermission period is delayed by its photo-dissociation process that occurs efficiently because of the overwhelmingly large number of photons [see

Eq. (4)] with energies in excess of the deuteron binding energy $E_d = 2.22$ MeV. Once the temperature drops to $T_9 \simeq 0.85$, the exponential Boltzmann suppression of such photons is sufficient to build a number density in D that is large enough to ignite other nuclear reactions. At these temperatures, the neutron-to-proton ratio has dropped to approximately 1/7 and very quickly, all neutrons are consumed and are incorporated into ${}^4\text{He}$ nuclei that have the highest binding energy per nucleon among all isotopes lighter than carbon. Thus, to a rather good accuracy,

$$Y_p \simeq \frac{2n/p}{1 + n/p} \Big|_{T_9 \simeq 0.85}. \quad (8)$$

The ${}^4\text{He}$ mass fraction Y_p is very weakly dependent on η_b as well as on the precise values for almost all nuclear reaction rates. Instead, Y_p is sensitive on the *timing* of major BBN events, such as the neutron-to-proton freeze-out and the end-point of the D bottleneck. Consequently, the prediction for Y_p relies on such well-measured quantities as the Newton constant, the neutron-proton mass difference, the Fermi constant, the neutron lifetime and the deuteron binding energy. The sensitivity of ${}^4\text{He}$ to all possible non-standard scenarios that modify the timing of BBN events causes this isotope to serve as the BBN “chronometer” [9]. SBBN predicts Y_p with an impressive precision (much better than 1%) so that the error bar is dominated by the uncertainty in the neutron lifetime.

The determination of primordial ${}^4\text{He}$ has been carried out by several groups [23, 24]. Such determination is performed via observations of hydrogen- and helium-emission lines in extragalactic HII-regions of low metallicity. Although the statistical error on Y_p —due to a large number of such observations—can be driven down to a $\mathcal{O}(10^{-3})$ -level, the extraction of the primordial value is limited by systematic errors [25]. Indeed, the latter errors are much larger than both, the statistical error and the accuracy of the SBBN prediction. We quote the most conservative analysis by Olive & Skillman [25], together with a recent update on the SBBN prediction [22],

$$\text{SBBN :} \quad Y_p = 0.2486 \pm 0.0002 \quad (9)$$

$$\text{extrapolation to primordial value :} \quad Y_p = 0.249 \pm 0.009. \quad (10)$$

Another recent analysis [26] finds a somewhat smaller error bar, $Y_p \simeq 0.250 \pm 0.004$, and for the purpose of this review we assume that the observational range for Y_p is limited to the range between 0.24 and 0.26. Clearly this error range is one of the most important issues in the application of BBN to particle physics, as it translates directly into the tightness of constraints on many non-standard scenarios. Further progress in understanding the error budget in the extraction of the primordial value of Y_p is needed.

1.1.2 $\mathcal{O}(10^{-5})$ ABUNDANCES: D AND ${}^3\text{He}$. Rapid formation of D at $T_9 \sim 1$ is counter-balanced by the uptake of helium producing reactions. Below $T_9 \sim 0.8$ the neutron-supply for D quickly drops in abundance, producing a characteristic peak in the D/H ratio as a function of temperature, Figure 1. The near complete burning of D then results in a rather small freeze-out value on the order of $\text{few} \times 10^{-5}$. Likewise, ${}^3\text{He}$ has a similar abundance to

D. BBN predictions for both elements are very sensitive to nuclear reaction rates as well as to the η_b -input. Nuclear reaction rates relevant for the formation of ${}^3\text{He}$ and D have been well measured to better than 10% accuracy. Therefore, by use of the current WMAP input, SBBN can make a fairly precise prediction for the abundances of these elements [22]:

$$\text{SBBN : } \quad \text{D/H} = 2.49 \pm 0.17 \times 10^{-5} \quad (11)$$

$$\text{SBBN : } \quad {}^3\text{He/H} = (1.00 \pm 0.07) \times 10^{-5}. \quad (12)$$

D can be observed in the local Universe as well as in highly redshifted clouds at low metallicities. The latter, see Refs. [27, 28, 29, 30, 31], is the preferred way of determining its primordial fraction. The observations of D absorption lines in quasar absorption systems (QALS) is challenging given that only a tiny isotopic shift separates the D line from the main hydrogen line. Only in a few cases of QALS with sufficiently simple velocity structure has the D/H ratio been extracted. The scatter of those resulting D/H determinations poses a certain problem because it exceeds the naively averaged error bar. Artificially inflating the errors in order to account for this scatter produces the following result [31]:

$$\text{QALS observations : } \quad \frac{\text{D}}{\text{H}} = (2.82 \pm 0.21) \times 10^{-5}. \quad (13)$$

This range agrees remarkably well with the SBBN prediction using the WMAP η_b -input. Despite the agreement one should be apprehensive of two potential problems. First, the galactic evolution of deuterium presents astronomers with a number of puzzles and implies some significant degree of absorption of D onto dust grains (For recent discussions, see for instance [32, 33]). Do similar mechanisms exist at QALS, and if so, should they result in an upward correction to Eq. (13) that would reflect the true primordial value of D/H? Second, the origin of scatter in the QALS data is not explained and could be a sign of underestimated systematic errors *or* additional depletion mechanisms. Until these issues are better understood, primordial values as high as 4×10^{-5} cannot be convincingly ruled out.

Unlike D, which can be depleted only in the course of the galactic evolution, both production and depletion of ${}^3\text{He}$ may occur; therefore, a direct interpretation of ${}^3\text{He}/\text{H}$ measurements as primordial is not possible. However, given the uni-directional evolution of D, one can conclude that the ${}^3\text{He}/\text{D}$ ratio will only grow thereby providing us with a very important *upper* bound on the primordial ${}^3\text{He}/\text{D}$ ratio [34]. For the purpose of this review, the primordial ratio can be constrained as [35]

$$\text{observational bound : } \quad \frac{{}^3\text{He}}{\text{D}} < 1, \quad (14)$$

which does not challenge SBBN, but rather represents an important constraint on non-standard BBN scenarios.

1.1.3 $\mathcal{O}(10^{-10})$ ABUNDANCES: ${}^7\text{Li}$. The formation of $A = 6, 7$ nuclei is suppressed in SBBN due to the absence of stable $A = 5$ elements. Tritium- α and ${}^3\text{He}$ - α fusion generates ${}^7\text{Li}$ and ${}^7\text{Be}$ nuclei, but with rates that are much smaller than the Hubble expansion rate.

Consequently, only a tiny number, $\text{few} \times 10^{-10}$ of ${}^7\text{Li}$ and ${}^7\text{Be}$ nuclei relative to hydrogen is generated. At a later stage of cosmological evolution ${}^7\text{Be}$ is ultimately converted into ${}^7\text{Li}$ via electron capture. At the WMAP-measured value of the baryon-to-photon ratio η_b , more than 90% of the primordial lithium is produced in the form of ${}^7\text{Be}$ in the radiative capture process, ${}^4\text{He} + {}^3\text{He} \rightarrow {}^7\text{Be} + \gamma$. The output of ${}^7\text{Be}$ is almost linearly dependent on the corresponding S -factor for this reaction, which was recently re-measured by several groups [36, 37, 38]. The current $\sim 15\%$ accuracy prediction for the combined ${}^7\text{Be} + {}^7\text{Li}$ abundance stands at [22]

$$\text{SBBN : } \frac{{}^7\text{Li}}{\text{H}} = 5.24_{-0.67}^{+0.71} \times 10^{-10}. \quad (15)$$

The discrepancy between this prediction and observations is often referred to as the lithium problem.

Due to its very low abundance, lithium cannot be determined from observations of extra-galactic absorption clouds. Instead, all observations of the ${}^7\text{Li}/\text{H}$ ratio must be performed in the atmospheres of low-metallicity galactic halo stars. The near constancy of ${}^7\text{Li}/\text{H}$ ratios at a low- but wide range of metallicities and for some range of effective stellar temperature is called the ‘‘Spite plateau’’. For a long time this plateau was thought to be an accurate representation of the primordial lithium abundance. A rather small scatter along the Spite plateau supports the interpretation of the measured ${}^7\text{Li}$ values as primordial. Although there have been numerous determinations of the ${}^7\text{Li}$ abundance on the Spite plateau, the most recent observations seem to indicate some metallicity-dependence of the ${}^7\text{Li}$ abundance. Furthermore, scatter may not be negligible, but rather may favor some amount of stellar ${}^7\text{Li}$ depletion [39, 40]. Currently, the observational status of the primordial lithium abundance is given by [41, 42]

$$\text{Spite plateau value : } \frac{{}^7\text{Li}}{\text{H}} = 1.23_{-0.16}^{+0.34} \times 10^{-10}, \quad (16)$$

which is a factor of three to five *lower* than the SBBN-predicted amount of primordial lithium, Eq. (15). It is important to keep in mind that measurements of lithium in globular clusters have resulted in somewhat higher abundances of $(2.19 \pm 0.28) \times 10^{-10}$ [42] (for other observational determinations of the ${}^7\text{Li}$ abundance consistent with [41, 42] see [43, 44]). The explanation of the discrepancy between (15) and (16) could be of purely astrophysical origin. [A potential additional depletion of SBBN values would require some un-orthodox modifications of secondary ${}^7\text{Be}$ -destroying reactions [45, 46]—but so far this possibility has not found support from nuclear experiments [47]]. Atmospheric ${}^7\text{Li}$ may have been partially depleted from atmospheres of population II stars due to additional settling mechanisms. Also, it has been suggested that stellar models that assume a factor ≈ 2 suppression of ${}^7\text{Li}$ in such stars, are consistent with observations of other abundances [48, 49]. Finally, it is also conceivable that the lithium problem points directly towards physics beyond the SBBN model, perhaps related to new physical processes at $T_9 \sim 0.5$. Unfortunately, given the controversial status of ${}^7\text{Li}$ it is difficult to use this isotope for constraining models of

new physics that modify its abundance. Instead, we point to certain interesting new physics possibilities that might be responsible for the reduction of ${}^7\text{Li}/\text{H}$.

1.1.4 $\mathcal{O}(10^{-14})$ AND LESS ABUNDANCES: ${}^6\text{Li}$ AND $A \geq 9$ ELEMENTS. ${}^6\text{Li}$ is the only stable $A = 6$ element. The main SBBN reaction that produces it,



is suppressed by four orders of magnitude relative to other radiative capture reactions such as ${}^4\text{He} + \text{T} \rightarrow {}^7\text{Li} + \gamma$, and is suppressed by approximately seven to eight orders of magnitude relative to other photonless nuclear rates. The reason for the extra suppression is unique as it arises from almost the same charge-to-mass ratio for ${}^4\text{He}$ and D, which inhibits the E1 transition, thereby making this radiative capture extremely inefficient. At the same time, the proton reaction that destroys ${}^6\text{Li}$ is very fast which leads to a $\mathcal{O}(10^{-14})$ -level prediction for primordial ${}^6\text{Li}$. This is well below modern detection capabilities. Heavier elements with $A \geq 9$ such as ${}^9\text{Be}$, ${}^{10}\text{B}$ and ${}^{11}\text{B}$ are never produced in significant quantities in the SBBN framework because of the absence of stable $A = 8$ nuclei, as ${}^8\text{Be}$ is under-bound by 92 keV and decays to two α particles.

Detections of ${}^9\text{Be}$, ${}^{10}\text{B}$, and ${}^{11}\text{B}$ have been made for many stars at low metallicities and are not controversial. Observations of ${}^9\text{Be}$ [50,51] are far above the $\mathcal{O}(10^{-18})$ SBBN prediction and exhibit a linear correlation with oxygen, clearly indicating its secondary (spallation) origin [52]. The lowest level of detected ${}^9\text{Be}/\text{H}$ is at $\sim \text{few} \times 10^{-14}$, which translates into a limit on the primordial fraction of 2×10^{-13} [53], assuming that there is no significant depletion of ${}^9\text{Be}$ in stellar atmospheres.

Because SBBN predicts very low ${}^6\text{Li}$ abundances, it is usually assumed that the origin of this isotope is not associated with BBN. Conversely, any level of ${}^6\text{Li}$ detection in stars at low metallicity in excess of $\mathcal{O}(10^{-12})$ is of interest for the test of both the SBBN framework and the galactic chemical evolution models. Remarkably, the existence of a ${}^6\text{Li}$ plateau at an isotopic ratio of ${}^6\text{Li}/{}^7\text{Li} \simeq 0.05$ has been claimed from (2σ) detections in approximately ~ 10 low-metallicity stars [44]. This level of ${}^6\text{Li}/{}^7\text{Li}$ should be considered high as it cannot be explained by cosmic ray production at such low metallicities [54]. However, in the thermal environment of stellar atmospheres the absorption lines of ${}^7\text{Li}$ and ${}^6\text{Li}$ are blended together so that observations become extremely challenging. Indeed, recent works [55] have claimed that additional convective motion in stellar atmospheres may lead to an ${}^6\text{Li}$ -unrelated distortion of ${}^7\text{Li}$ absorption lines which could be confused with positive ${}^6\text{Li}$ -detections. The analysis by Cayrel *et al.* [55] favors the latter explanation and sets a number of upper limits on the ${}^6\text{Li}/{}^7\text{Li}$ in several stars of interest.

We now move to the main topic of our paper: modification of BBN by new physics. Instead of concentrating on very specific models of particle physics and/or gravitation, we review different *classes* of models that modify or abandon the main assumptions of SBBN listed in the Introduction.

2 NEW PHYSICS AFFECTING THE TIMING OF MAIN BBN EVENTS

As shown in Figure 1, most neutrons are incorporated into ${}^4\text{He}$ at a very specific moment: the end of the D bottleneck. The amount of helium and deuterium that results has a strong dependence on the n/p ratio that, in turn, translates into a sensitivity to a much earlier event in the BBN history: the freeze-out of neutron-to-proton interconversion. Different physical processes may affect the timing of both events and thereby change the BBN output.

2.1 BBN with new degrees of freedom

A classic application of BBN consists of constraining the number of the excited relativistic degrees of freedom. Traditionally, this procedure is formulated in terms of a constraint on the effective number of neutrino species, $N_{\nu,\text{eff}}$. To be more general, we re-formulate such a bound as a limit on the amount of so-called “dark radiation”, ρ_{dr} . By dark radiation we mean extra massless or nearly-massless degrees of freedom that have the expected scaling as the Universe expands, $\rho_{dr} \sim a^{-4}$. Furthermore, we assume that this additional relativistic component is totally “passive” and that it does not exchange energy with any SM species. This viewpoint can then be easily applied to the thermally decoupled extra bosonic or fermionic degrees of freedom. The addition of dark radiation to the cosmic energy budget amplifies the Hubble expansion rate,

$$H_{\text{SBBN}} \rightarrow H = H_{\text{SBBN}} \sqrt{1 + \rho_{dr}/\rho_{\text{SM}}}, \quad (18)$$

leading to an *earlier* freeze-out of the n/p ratio and thus to a larger helium mass fraction. In this formula, ρ_{SM} and H_{SBBN} are the SBBN energy density and the Hubble rate, respectively. Figure 2 illustrates the changes to the abundances of helium, deuterium and lithium as a function of $\rho_{dr}/\rho_{\text{SM}}$ and shows that even the somewhat generous assumption on the error bar of Y_p translates into a rather tight constraint on ρ_{dr} . One cannot achieve any significant degree of ${}^7\text{Li}$ suppression without violating other bounds. Figure 2 formally extends to the region of negative ρ_{dr} . This may seem unphysical, but a negative ρ_{dr} effect can be mimicked by models with decreased neutrino temperatures due to, for instance, additional electromagnetic energy injection at approximately $T \sim 2$ MeV. Assuming that ${}^4\text{He}$ is limited to the range between 0.24 and 0.26, one arrives at the conclusion that

$$-0.06 < \frac{\rho_{dr}}{\rho_{\text{SM}}} < 0.14. \quad (19)$$

Presented in a traditional way, this constraint corresponds to $2.6 \lesssim N_{\nu,\text{eff}} \lesssim 4$.

The constraint on ρ_{dr} can be further specified to models at hand. It can be applied to limit the energy density carried by very light and thermally decoupled scalar fields. For example, if the dark energy sector at the time of BBN corresponds to a very light classical scalar field ϕ that tracks ρ_{SM} [56, 57], Eq. (19) constrains the parameters of the potential, $V(\phi)$. For an exponential potential of the form $V(\phi) = M^4 \exp\{-\lambda\phi/M_{Pl}\}$, the energy density carried by the tracker field is $\rho_\phi/\rho_{\text{total}} = 4/\lambda^2$, so that the magnitude of λ should be larger approximately five so as to satisfy (19).

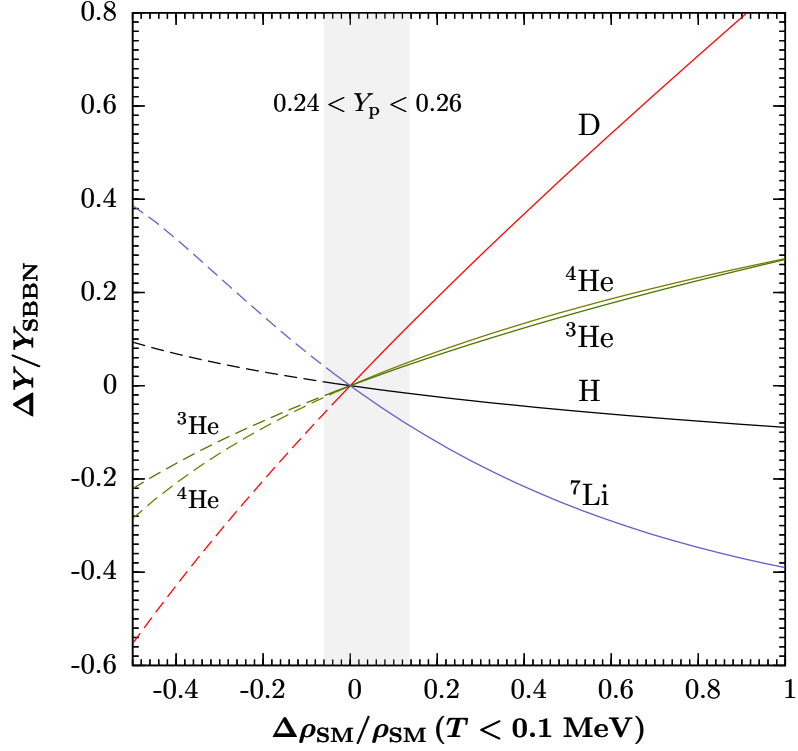


Figure 2: Change of nuclear abundances relative to their SBBN values as a function of the “dark radiation” component $\rho_{dr}/\rho_{SM} = \Delta\rho_{SM}/\rho_{SM}$. The vertical band shows the allowed amount of dark radiation that keeps Y_p in the $0.24 \div 0.26$ window.

The result (19) can also be developed further into constraints on the *properties* of the dark radiation fields and the temperature of their thermal decoupling from the SM field content. Suppose that the dark radiation sector contains N bosonic light neutral fields that are connected to the SM via some heavy Λ_n -scale suppressed operators of dimension $n > 4$. Then, the thermalization rate of dark radiation with the SM particles would typically scale as $\Gamma_{th} \sim T(T/\Lambda_n)^{2(n-4)}$. The temperature of thermal decoupling is given by the condition $H(T_d) \sim \Gamma_{th}$. Therefore, for every given N that threatens to violate the bound of Eq. (19) one can determine a *minimal* decoupling temperature, and for any given n place a *lower* bound on the high-energy scale Λ_n . For example, if $N \geq 3$, then the thermal decoupling of these species must occur around the quantum chromodynamics hadronization epoch ($T \sim 200$ MeV) or earlier. By comparing the Hubble rate with the thermalization rates at that epoch, one arrives at

$$N \geq 3 \Rightarrow \Lambda_5 > 5 \times 10^8 \text{ GeV}; \Lambda_6 > 5 \text{ TeV}. \quad (20)$$

If the interaction is mediated by dimension five operators then the sensitivity to the Λ scale can extend very far—indeed, much beyond directly accessible energy scales in collider experiments. In exactly the same way, one can constrain properties and interactions of right-handed neutrinos, should they be light. For example, Eq. (19) can be used to set

limits on the strength of the coupling between left- and right-handed neutrino species. Finally, even if the right-handed neutrinos are heavy and not excited, BBN allows one to constrain non-standard properties of the left-handed neutrino species. For example, a sizable magnetic moment or charge radius of neutrinos (that correspond to dimension five and six effective interactions with the external electromagnetic current) may be strong enough to prolong the thermal coupling of neutrinos to the electron-positron-photon fluid, thereby leading to essentially higher T_ν than predicted by the standard scenario (7). More discussions on the status of BBN with extra degrees of freedom can be found in earlier reviews [6, 7, 8, 9].

2.2 BBN with sliding couplings and mass scales.

An alternative, and more exotic way to affect the timing of main BBN events is realized in models that predict a time evolution of coupling constants and mass scales. A tractable version of such models represents a Brans-Dicke-type scalar field that couples to the SM operators $F_{\mu\nu}^2$ and $m_q \bar{q}q$ where m_q is a quark mass. The evolution of the scalar field creates the effect of changing m_q , electric charge, Λ_{QCD} , Higgs vacuum expectation value, and so forth. These changes, in turn, induce changes in the reaction rates, nuclear binding, and the position of resonances. Much effort has been devoted to calculations that make such connections explicit [58, 59]. Several works have addressed the question of coupling variability in connection to BBN; for the most recent accounts, we refer the reader to, for instance [60, 61, 62, 63].

Rather than delve into the intricacies of coupling and the scale dependence of nuclear parameters, we limit ourselves to the following simplified framework. We assume that the primary effect of the change of couplings is on the value of the neutron-proton mass difference Δm_{np} and on the deuteron binding energy E_d . We disregard other possible changes, *i.e.* in the Coulomb barrier penetration, shifts in the position of nuclear resonances etc. Such an approximation is somewhat justified because both, Δm_{np} and E_d , enter in the exponents that control (a) the n/p ratio around its freeze-out time and (b) the D abundance around the end of the bottleneck. By using this approach, we are certain to capture the main effects related to the change of couplings because Δm_{np} influences the n/p freeze-out and the value of E_d dictates the end of the D bottleneck. Moreover, the deuteron binding energy is among the most sensitive nuclear parameters to the variation of m_q/Λ_{QCD} due to a strong cancellation of m_q -dependent against m_q -independent components in the deuteron binding energy [61].

Figure 3 shows contours of D, ^4He and ^7Li abundances in the $\Delta m_{np}-E_d$ plane when both variations are implemented simultaneously. The abundances of elements are very sensitive to the variations of these quantities: helium in particular is extremely sensitive to Δm_{np} . Moreover, among all elements, lithium appears to be the most sensitive to the variation of the deuteron binding energy because for smaller values of E_d , the end of the D bottleneck is delayed, and the $^3\text{He}(\alpha, \gamma)^7\text{Be}$ reaction is even less efficient than in SBBN. The possibility

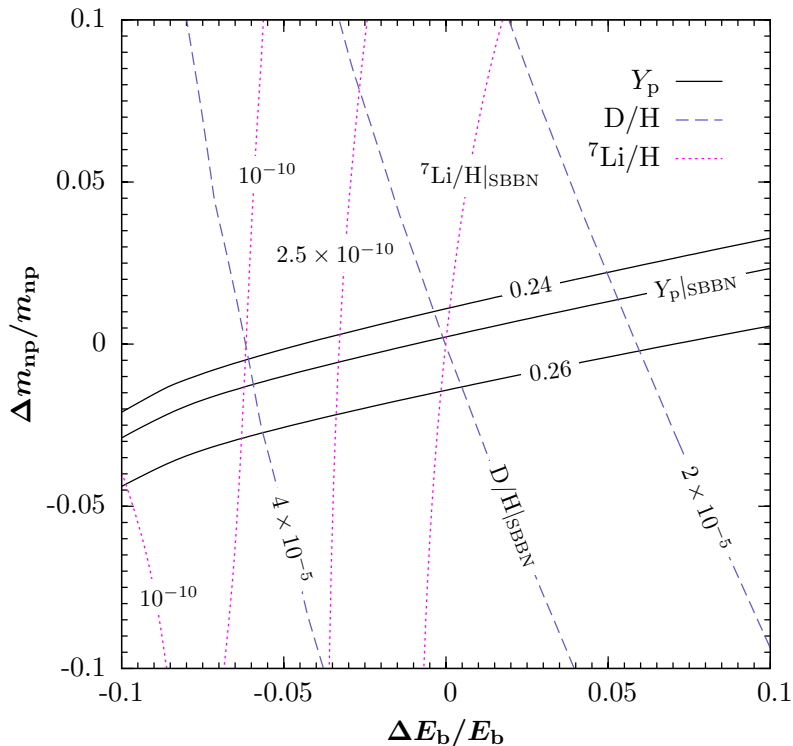


Figure 3: Contours of Y_p , D/H and ${}^7\text{Li}/H$ are plotted in the parameter space of variable neutron-proton mass difference Δm_{np} and deuteron binding energy E_d , normalized to their current values. The 5-10% downward change in E_b can significantly reduce ${}^7\text{Li}$ abundance.

of suppressing the lithium abundance while maintaining the agreement with helium and deuterium was noted in recent papers [61, 62, 63]. A rather strong sensitivity of E_d to the m_q/Λ_{QCD} parameter ensures that even a small variation of the latter leads to a drastic change in lithium.

3 NON-EQUILIBRIUM BBN

One of the main assumptions of standard BBN is that all reactions occur between partners that are perfectly thermalized with the photon background fluid. However, even the standard nuclear processes that occur during BBN lead to a non-thermal energy component which is released when mass is converted into nuclear binding energy. It is easy to estimate how much of this energy is injected. Because the total binding energy of helium is 28 MeV, the total energy release is just under 2 MeV per nucleon. Although such an energy injection is noticeable when it occurs later in the history of the Universe, the release of such energy at $T_9 = 0.85$ does not lead to a change in SBBN predictions (for an analysis of some SBBN non-equilibrium reactions see Ref. [64]).

More drastically, non-standard decaying or annihilating particles can also increase the energy release per nucleon. Indeed, if this occurs predominantly after nucleosynthesis is

complete it can lead to strong departures from the observed pattern of primordial abundances. Therefore, BBN provides us with a significant sensitivity to this class of models even when the total energy density stored in the decaying and annihilating species is completely subdominant to the energy density of the Universe. This issue has taken on a great deal of importance due to its potential connection to particle dark matter, in which weakly interacting massive particles (WIMPs) can either source non-equilibrium BBN via their annihilation, or be produced in the decays of some metastable parent particles.

BBN scenarios with additional energy injection have received a plenty of attention since their inception [65,66,67,68,69,70,71,72], more recent and more detailed treatments can be found in [73,74,75,76,77]. By accounting for the qualitative differences in the abundance signatures, one may distinguish between electromagnetic decays to γ s, e^\pm , and possibly other leptons and decays to hadronic final states that lead to extra energetic nucleons. Whereas electromagnetic decays have a significant impact on BBN only at late times ($\tau \gtrsim 10^5$ s), after all reactions are effectively frozen, the hadronic decays may have observable consequences even if they occur as early as few seconds.

3.1 BBN with electromagnetic and hadronic energy injection

When the decaying particle produces mostly electromagnetic radiation, the treatment of non-equilibrium BBN is relatively simple. Because the density of the early Universe is quite significant, decaying particles quickly yield electromagnetic showers. As a result, a potentially very large energy release per decaying particle (*i.e.* $\mathcal{O}(1$ TeV) can be transferred to a large number of $\mathcal{O}(10$ MeV)-energy photons, some of which may have a chance of interacting with and/or disintegrating light nuclei before their energy is further dispersed and thermalized.

The main physical process that regulates the *maximal* energy of particles in the shower is the pair-production in the scattering of energetic γ s on thermal photons, *i.e.* $\gamma + \gamma_T \rightarrow e^- + e^+$. This leads to a so-called “zeroth-generation” differential photon spectrum in the form of a broken power law [78]:

$$p_\gamma(E_\gamma) = \begin{cases} K_0(E_\gamma/E_{\text{low}})^{-1.5} & \text{for } E_\gamma < E_{\text{low}} \\ K_0(E_\gamma/E_{\text{low}})^{-2.0} & \text{for } E_{\text{low}} < E_\gamma < E_C \\ 0 & \text{for } E_\gamma > E_C \end{cases} \quad (21)$$

where the power break occurs at $E_{\text{low}} \simeq m_e^2/(80T)$, and the spectrum is cut-off at the threshold of pair production $E_C \simeq m_e^2/22T$ [72]. The overall normalization constant K_0 of the spectrum is determined by requiring that the primary injected (electromagnetic) energy E_0 be carried by the photon cascade, that is, $E_0 = \int dE_\gamma E_\gamma p_\gamma$.

The ansatz (21) for the spectrum immediately tells us the temperature and time of injection that allow for the photodisintegration of a certain element. The highest temperature T_{ph} (one-to-one related to the earliest cosmological time) at which photodisintegration can

occur can be determined by equating E_C to the nuclear binding energies E_b against photodissociation:

$$T_{\text{ph}} \simeq \begin{cases} 7 \text{ keV} & \text{for } {}^7\text{Be} + \gamma \rightarrow {}^3\text{He} + {}^4\text{He} & (E_b = 1.59 \text{ MeV}) \\ 5 \text{ keV} & \text{for } \text{D} + \gamma \rightarrow n + p & (E_b = 2.22 \text{ MeV}) \\ 0.6 \text{ keV} & \text{for } {}^4\text{He} + \gamma \rightarrow {}^3\text{He}(\text{T}) + n(p) & (E_b \simeq 20 \text{ MeV}) \end{cases} \quad (22)$$

Once the temperature is so low that the photodisintegration of ${}^4\text{He}$ can occur, net *production* of D and ${}^3\text{He}$ becomes possible. An amount of ${}^6\text{Li}$ can be produced either via photodissociation of ${}^7\text{Be}$ and ${}^7\text{Li}$ or through secondary interactions of the products of ${}^4\text{He}$ destruction. This important mechanism is discussed in some detail later.

The photons in the cascade (21) undergo further degradation via the (slower) processes of Compton scattering, pair-production on nuclei, and elastic γ - γ scattering so that the total number of energetic photons is given by competition between the injection (decay or annihilation) rate Γ_{inj} and the total energy loss rate $\Gamma_\gamma(E_\gamma)$. The energy spectrum can then be obtained in form of a quasi-static equilibrium solution [79]

$$f_\gamma^{\text{qse}} = n_X \frac{\Gamma_{\text{inj}} p_\gamma(E_\gamma)}{\Gamma_\gamma(E_\gamma)}, \quad (23)$$

where n_X is the time-dependent number density of the decaying and annihilating particles, $\Gamma_{\text{inj}} = \tau_X^{-1}$ for decays, and $\Gamma_{\text{inj}} = \frac{1}{2} n_X \langle \sigma_{\text{ann}} v \rangle$ for self-annihilation. Depending on the temperature of the primordial plasma at the time of energy injection, both production and destruction of elements may occur. One can incorporate these possibilities into an additional set of Boltzmann equations, which include the non-thermal photon population and abundances of nuclei denoted here as T , A , and P ($A_T > A_A > A_P$):

$$\begin{aligned} -HT \frac{dY_A}{dT} &= \sum_T Y_T \int_0^\infty dE_\gamma f_\gamma^{\text{qse}}(E_\gamma) \sigma_{\gamma+T \rightarrow A}(E_\gamma) \\ &\quad - Y_A \sum_P \int_0^\infty dE_\gamma f_\gamma^{\text{qse}}(E_\gamma) \sigma_{\gamma+A \rightarrow P}(E_\gamma). \end{aligned} \quad (24)$$

The solution to this set of equations constrains the amount and timing of deposited electromagnetic energy. Figure 4 shows the results of a sample calculation for the model with a decaying particle with a lifetime of $\tau_X = 10^8 \text{ s}$ and an initial energy density relative to baryons of $m_X n_X / (m_p n_b) = m_X Y_X / m_p \simeq 1$; there is an extra assumption that half of the rest mass of the species, $m_X = 1 \text{ TeV}$, is released in the form of electromagnetic energy into the thermal bath. One can see the significant increase in ${}^3\text{He}$, D, and ${}^6\text{Li}$ abundances. The solid arrows indicate the main transformations of the elemental abundances under the influence of the dissociating radiation. The model considered in this graph is in stark conflict with observations and is therefore excluded.

It is intriguing to investigate whether the injection of electromagnetic energy may reduce the abundance of ${}^7\text{Li} + {}^7\text{Be}$. A dedicated study [80] found that such a reduction is generally difficult to achieve because either D is also destroyed or ${}^3\text{He}/\text{D}$ is overproduced beyond

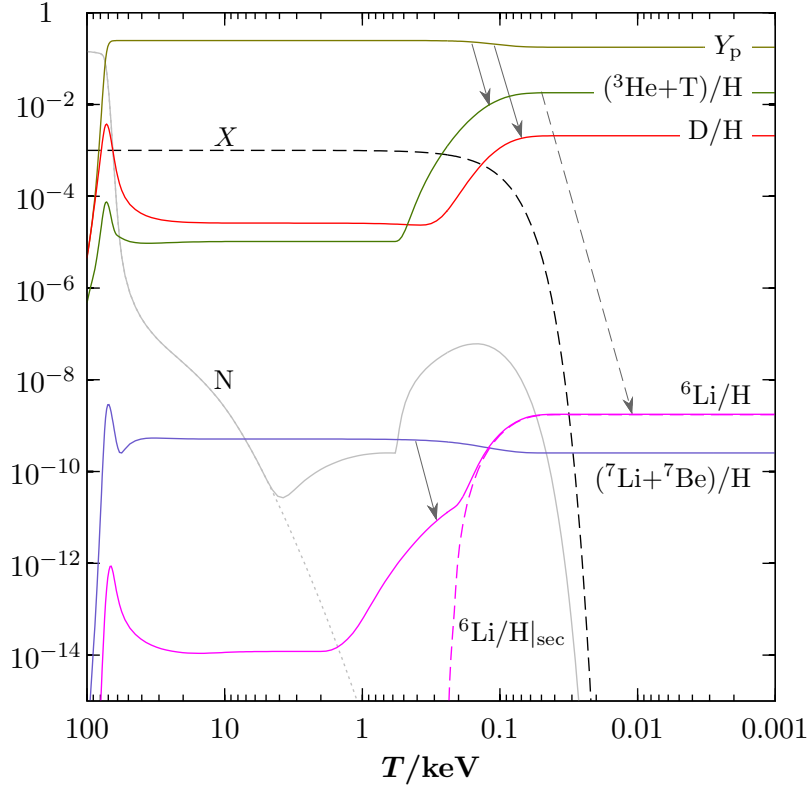


Figure 4: Consequences of late decays of a heavy 1 TeV mass particle X that releases half of its rest mass in the form of electromagnetic energy. The threshold of ${}^4\text{He}$ disintegration is clearly visible below 1 keV. Primary abundance flows are indicated by solid arrows whereas the dashed arrow indicates the secondary transformation of $A = 3$ nuclei into ${}^6\text{Li}$. The model is excluded by the overproduction of D , ${}^3\text{He}$, and ${}^6\text{Li}$.

observationally acceptable levels. Although the overall conclusion is negative, *i.e.* the electromagnetic destruction of ${}^7\text{Li}$ is problematic, we stress that “just-so” solutions can always be found. For example, consider a relatively light but abundant neutral particle with mass m in the narrow range between ~ 3.5 and 4.5 MeV. ${}^7\text{Be}$ could indeed be destroyed while D , ${}^3\text{He}$, and ${}^6\text{Li}$ remain unaffected because the maximum released energy, $m/2$, lies below their photo-disintegration threshold.

The treatment of energy injection via hadronic channels is significantly more complicated because additional effects must be taken into account. Partons emitted in a decay or annihilation are quickly hadronized and the highly energetic fragmentation products [mostly pions but also (anti-)nucleons] are released into the plasma. Only long-lived mesons—namely, charged pions (π^\pm) and kaons (K^\pm , K_L^0)—with lifetimes of $\mathcal{O}(10^{-8}$ s) have a chance to interact with background nuclei before decaying. A very early hadronic energy injection ($300 \text{ keV} \lesssim T \lesssim 1 \text{ MeV}$) allows the π -mesons to participate in charge exchange reactions, $\pi^- + p \rightarrow \pi^0 + n$. Such reactions lead to a higher n/p freeze-out value, thereby increasing the helium mass fraction Y_p . Similar effects can be caused by anti-nucleons, which tend

to annihilate predominantly on protons. The most important difference with respect to electromagnetic energy releases comes from the injection of energetic nucleons after the formation of ${}^4\text{He}$. The propagation of energetic nucleons through the primordial plasma causes spallation processes on ${}^4\text{He}$. Reactions caused by energetic nucleons— $n + {}^4\text{He} \rightarrow \text{T} + p + n$, $n + {}^4\text{He} \rightarrow \text{D} + p + 2n$ and others—in turn generate energetic $A = 3$ elements that can participate in endo-thermic nuclear reactions that are forbidden in SBBN.

What determines the efficiency of spallation processes and of subsequent secondary non-thermal reactions is the rate at which the energetic charged nuclei and neutrons are stopped by the primordial plasma. The dominant thermalization processes for charged nuclei are Coulomb interactions with e^\pm and Thomson scattering off thermal photons. Below the e^+e^- annihilation threshold the stopping power of the plasma rapidly drops with temperature, reaching its minimum at approximately $T \simeq 20$ keV. The energy loss of the neutrons initially occurs via its magnetic-moment interaction with electrons and positrons. At later stages ($T \lesssim 80$ keV), neutrons lose their energy dominantly by scattering on protons and ${}^4\text{He}$.

The resulting constraints on energy injection are described in great detail elsewhere [73, 74, 75, 76, 77]. BBN results are most sensitive to the energy injection after 10^8 s, where constraints as strong as ~ 1 MeV per nucleon result from the secondary ${}^6\text{Li}$ production, and do not generally depend on the branching ratio to hadrons. Constraints on electromagnetic energy injection depend, to a large extent, on whether ${}^4\text{He}$ can be photo-dissociated, and they become much weaker if energy is released when the temperature is above 0.6 keV. Hadronic decays allow one to probe much earlier times. For fully hadronic decays to energetic $q\bar{q}$ pairs, similar sensitivity (1 MeV per nucleon) applies to injection at much earlier times, specifically $t \sim 10^4$ s. Perhaps one of the most interesting features of energy injection with nucleons in the final state is the effect of extra neutrons at $T \sim 40$ keV, which may lead to an important depletion of the total lithium abundance.

3.1.1 NEUTRON EXCESS AT 40 KEV AND SUPPRESSION OF ${}^7\text{Li}$. An interesting aspect of non-thermal BBN with hadronic decays and annihilations is the possibility of alleviating the tension between the Spite plateau value and the predicted abundance of ${}^7\text{Li}$, *e.g.* “solve the ${}^7\text{Li}$ problem”. In SBBN the ${}^7\text{Be}$ abundance is controlled by the ${}^3\text{He} + {}^4\text{He} \rightarrow {}^7\text{Be} + \gamma$ reaction and by the combination of the two reactions that destroy it:



The increase of neutrons in a narrow temperature interval $60 \text{ keV} \gtrsim T \gtrsim 30 \text{ keV}$ (in other words, during or just after ${}^7\text{Be}$ synthesis) may amplify the efficiency of this destruction. The injection of $\gtrsim 10^{-5}$ neutrons per baryon, regardless the microscopic cause of such an injection, may enhance ${}^7\text{Be} \rightarrow {}^7\text{Li}$ and lead to an overall depletion of ${}^7\text{Be} + {}^7\text{Li}$ [68, 73]. When the temperature drops below 30 keV, the ${}^7\text{Li}$ burning reaction drops out of equilibrium, the lithium destruction stops, and the supply of “extra neutrons” has no further effects on the overall ${}^7\text{Be} + {}^7\text{Li}$ abundance. At the same time, most of the extra neutrons injected around the time of BBN are removed by the radiative recombination with protons leading

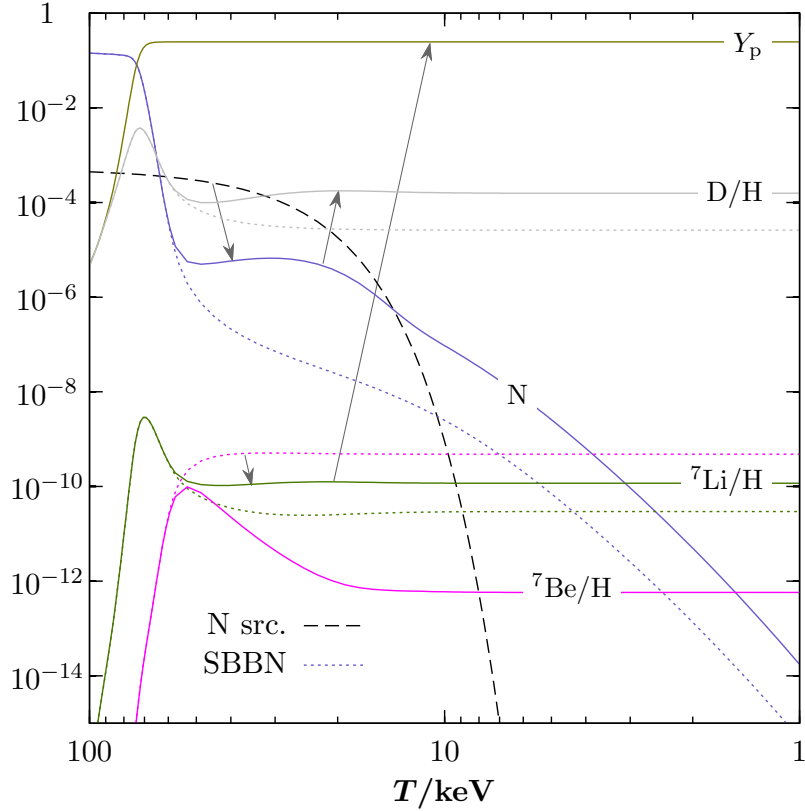


Figure 5: Effects on element abundances in response to an elevated (thermal) neutron content, sourced by a decaying species, at early times. Although neutrons are mostly incorporated into D, they also transfer ${}^7\text{Be}$ nuclei into the ${}^7\text{Li}$ reservoir from which they are more susceptible to proton burning. This mechanism suppresses the overall outcome of the $A = 7$ elements.

to the generation of extra D. Therefore, one should expect that this mechanism of depleting ${}^7\text{Be}$ is tightly constrained by the abundance of D. The temperature evolution of elemental abundances in the presence of an extra source of thermal neutrons is illustrated in Fig. 5.

Elevated neutron concentrations can be caused by decaying or annihilating particles that contain a significant number of baryons in the final state. This presence is amplified when the energetic particles lose their energy in collisions with the primordial plasma. Many details of such processes depend on concrete particle physics realizations: particle masses, abundances, lifetimes, branching ratios to nucleons, and so forth all play important roles. In Figure 6 we both emulate the process of energy injection by assuming very rapid thermalization and study the effect of extra neutrons on ${}^7\text{Li}+{}^7\text{Be}$ and D abundances by varying the amount of injected neutrons, while assuming different time (or temperature) patterns for such injections. Specifically, we include cases of decaying particles (with different lifetimes), and annihilating WIMPs, with or without possible Sommerfeld or resonant enhancement of annihilation [81]. If not carefully tuned, the injection of neutrons that reduces the total ${}^7\text{Li}$

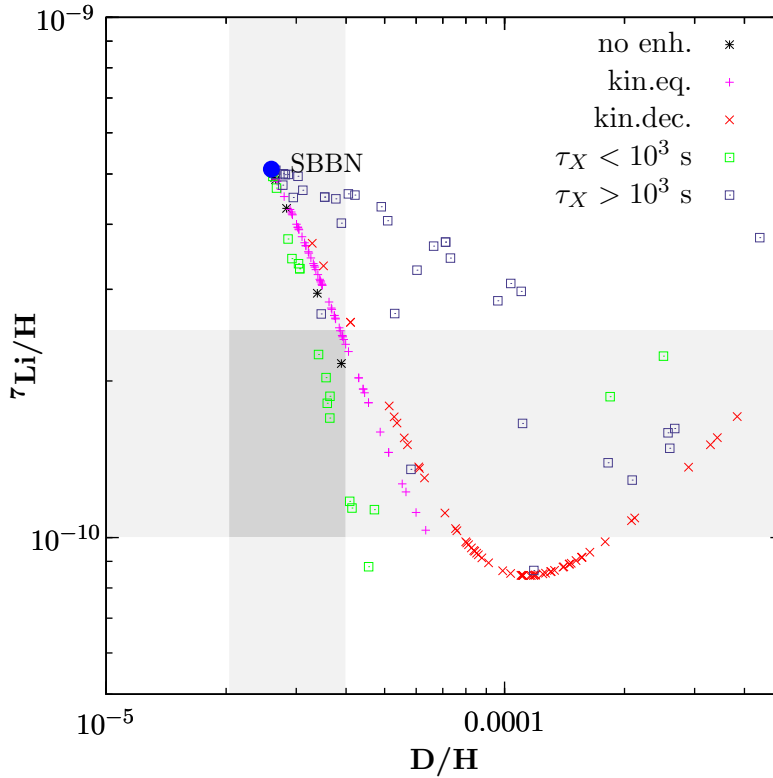


Figure 6: ${}^7\text{Li}$ versus D abundance in the BBN scenario with “extra” neutrons. The overall number of injected neutrons, as well as the temporal patterns of injection, is varied. Patterns consistent with particle decays and annihilation, both with and without Sommerfeld enhancement, are considered.

abundance by a factor of two, would over-predict the D/H ratio. Only a relatively small subset of models, typically those whose decaying particles have lifetimes below 1000 s are consistent with D/H, and provide enough suppression for ${}^7\text{Li}$. However, the injection of energetic neutrons, ignored in this treatment is also important because of secondary and tertiary reactions induced by the neutrons. These reactions lead to an increase of rare light elements such as ${}^6\text{Li}$ and ${}^9\text{Be}$. This method of correcting the lithium problem is subject to additional constraints from ${}^6\text{Li}$ and ${}^9\text{Be}$.

3.1.2 PRODUCTION OF ${}^6\text{Li}$, ${}^9\text{Be}$, AND ${}^{10}\text{B}$ IN SECONDARY COLLISIONS. As stated in the introduction, the abundances of these elements predicted by SBBN are extremely low. The path to them is heavily hindered as it is guarded by (a) the breaks at $A = 5$ and 8, (b) the low efficiency of the SBBN reaction (17) and (c) the efficient destruction of these elements by protons which stops only at $T \sim 10$ keV when the destruction rates fall below the Hubble expansion rate. Non-equilibrium BBN provides an important mechanism for circumventing at least some of that suppression through access to endo-thermic reactions that have much higher cross sections [67].

Energetic mass three nuclei, ${}^3\text{He}$ and tritium, produced via electromagnetic or hadronic

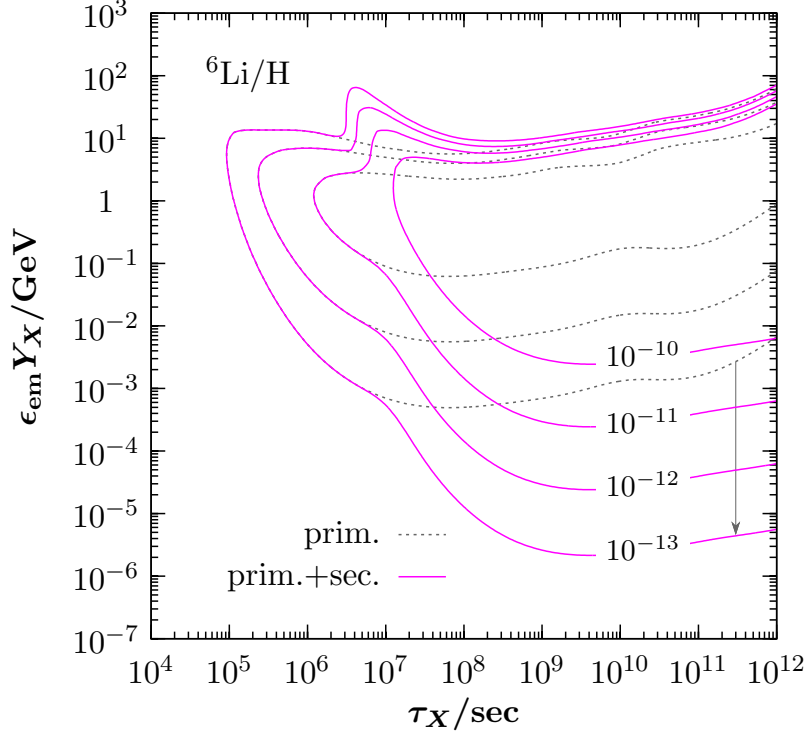
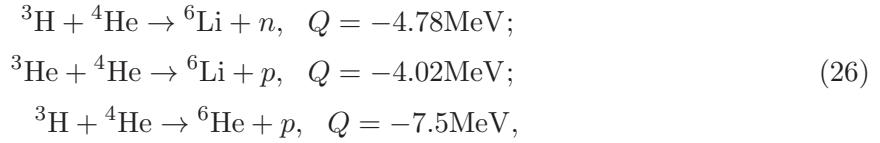


Figure 7: Contour lines of ${}^6\text{Li}/\text{H}$ in the plane of X-lifetime τ_X and total injected (electromagnetic) energy per baryon: $\epsilon_{\text{em}}Y_X$. Only below ~ 10 keV ($t > 10^4$ s) are ${}^7\text{Li}$ and ${}^7\text{Be}$ dissociated by energetic photons producing “primary” ${}^6\text{Li}$ (dotted lines). Additionally, ${}^6\text{Li}$ is fused via the processes of Eq. 26). The importance of this “secondary” production at late times represented by the vertical arrow which indicates the significant elevation of total ${}^6\text{Li}/\text{H}$ (solid lines) with respect to the primary yield (dotted lines).

energy injection (*i.e.* via spallation or photodisintegration) collide with α particles from the thermal bath. Such secondary collisions produce ${}^6\text{Li}$ via the following set of reactions.



where ${}^6\text{He}$ subsequently β -decays to ${}^6\text{Li}$. For energies of projectiles that are approximately 10 MeV, the cross sections for these non-thermal processes are on the order of 100 mb— 10^7 times larger than the SBBN cross section for the production of ${}^6\text{Li}$. The overall efficiency of producing ${}^6\text{Li}$ from energetic ${}^3\text{He}$ and tritium reaches its maximum at $\mathcal{O}(10^{-4} - 10^{-3})$ below $T = 10$ keV; therefore, even one energetic nucleus of tritium per one million protons can have a very significant impact on ${}^6\text{Li}$. This enhancement figure underscores the sensitivity of ${}^6\text{Li}$ to non-thermal BBN and makes it an important probe of energy injection mechanisms in the early Universe.

Figure 7 illustrates the importance of accounting for secondary reactions of the kind (26)

when tracking the ${}^6\text{Li}$ output in scenarios with electromagnetic energy release at late times. Shown are contour lines of constant ${}^6\text{Li}/\text{H}$ for varying lifetime τ_X of an decaying species X and different total injected (electromagnetic) energy per baryon, $\epsilon_{\text{em}}Y_X$. Whereas the dotted lines represent the “primary” abundance of ${}^6\text{Li}$ generated in the photodissociation of ${}^7\text{Li}$ and ${}^7\text{Be}$, its “secondary” production becomes very important as soon as $\tau_X \gtrsim 10^7$ s. This is highlighted by the vertical arrow indicating the increased sensitivity to a decaying species by three orders of magnitude, attributed to the secondary production mechanism. In our treatment of photodissociation processes we primarily follow the approach of Ref. [79].

The doubtful observational status of ${}^6\text{Li}$ and the possibility of its stellar depletion over and above the depletion of ${}^7\text{Li}$ should stimulate studies of ${}^9\text{Be}$ and boron production via the non-thermal nucleosynthesis. So far, this subject has escaped the attention of the groups working on non-equilibrium BBN. Note that *tertiary processes* may be responsible for the non-equilibrium ${}^9\text{Be}$ production. The ${}^6\text{He}$ and ${}^6\text{Li}$ nuclei emerging from secondary reactions (26) can collide further with particles from the bath,



and generate ${}^9\text{Be}$ from $A = 6$ nuclei with similar efficiencies to the $A = 3 \rightarrow A = 6$ transition. The actual output of ${}^9\text{Be}$ relative to ${}^6\text{Li}$ is enhanced beyond a crude estimate of $\mathcal{O}(10^{-4} - 10^{-3})$ if, for example, the energy injection occurs both at very early times and above $T = 12$ keV, where ${}^6\text{Li}$ is more rapidly destroyed by proton reactions than ${}^9\text{Be}$ is. Given the absence of a primordial ${}^9\text{Be}$ plateau down to the level of 10^{-13} , it is desirable to investigate the tertiary production mechanisms of beryllium and boron in more detail [82].

3.2 Energy injection by WIMPs

Decays of heavy relics may represent the simplest possible way to achieve energy injection. However, without specifying the model and the physical mechanisms that lead to the production of unstable particles and their subsequent decay, one cannot estimate the amount or the timing of the energy injection. In contrast, WIMPs represent a somewhat more restricted framework in which the leading mechanisms regulating the WIMP abundance at BBN time is their self-annihilation at earlier times. Assuming a weak-scale mass for a relic WIMP as well as a typical range for the annihilation cross section, one can deduce its abundance as a function of mass and annihilation rate. The most restrictive framework is that of stable neutral WIMPs that form the dominant component of cold dark matter. Although most of the WIMPs annihilate when the temperature drops below the WIMP mass, a residual annihilation persists even at BBN times [83]. The question of WIMP annihilation at early times, during BBN, is important in view of the attempts to detect signatures of WIMP annihilation in our own Galaxy. Indeed, a broad similarity among WIMP velocities inside the Galaxy and during BBN tells us that the kinematics of WIMP collisions must be very similar.

The most straightforward case to consider is a single species of WIMP dark matter X with annihilation rate $(\sigma v)_0 \simeq 3 \times 10^{-26} \text{cm}^3 \text{s}^{-1}$ averaged over the thermal bath at the freeze-out. Such an annihilation rate yields a total energy density of WIMPs that is close to what is required for cold dark matter by observations. This result provides us with a convenient normalization point for the annihilation rate at *arbitrary* WIMP velocities in the center-of-mass frame:

$$\sigma(v)v = S(v)(\sigma v)_0. \quad (28)$$

In the simplest case, in which the annihilation is mediated by short-distance forces and proceeds in the s -wave, the velocity dependence is trivial: $S(v) = 1$. The fraction of WIMPs that is still annihilating at the time of BBN during one Hubble time H^{-1} is given by

$$f_X(t_{\text{BBN}}) \simeq \left. \frac{\langle \sigma(v)v \rangle n_X}{H} \right|_{t=t_{\text{BBN}}} \quad (29)$$

where $\langle \dots \rangle$ denotes a thermal average that can be calculated once the velocity dependence of $S(v)$ and the thermal distribution of WIMPs are specified.

We are interested in finding the fraction of annihilating WIMP particles within a Hubble time at $T < 10 \text{keV}$, specifically, at a temperature scale below which ${}^6\text{Li}$ is no longer susceptible to nuclear burning in the ${}^6\text{Li}(p, \alpha){}^3\text{He}$ reaction. In general, this fraction can be expressed via the freeze-out temperature $T_f \sim 0.05 m_X$ and the number of effective degrees of freedom at an arbitrary temperature $T < T_f$ [10]:

$$f_X(T) \simeq \left[\frac{g(T)}{g(T_f)} \right]^{1/2} \frac{T}{T_f} \langle S(v) \rangle_T. \quad (30)$$

There are several generic options for the temperature scaling of the S -factor in (30). In the simplest case of $S(v) = 1$, one can use Eq. (30) to deduce that for a WIMP of mass $M_X = 100 \text{GeV}$ ($T_f \sim 5 \text{GeV}$) only a small fraction, $f_X \approx 6 \times 10^{-7}$, of the X -particles has the chance to annihilate at $T \simeq 10 \text{keV}$ and below. This corresponds to an injection of approximately 10^{-15}GeV per photon. Nevertheless, even this tiny fraction may be sufficient to produce a ${}^6\text{Li}$ abundance up to the 10^{-12} -level, provided that hadronic annihilation channels dominate. Lighter WIMPs may have a more pronounced effect on BBN [73]. Short-range mediated annihilation in the p -wave gives $S(v) \sim v^2$ and negligible energy release at BBN.

Much enhanced annihilation rates occur in models where interactions are mediated by an attractive Coulomb-like force and/or have near-threshold resonances. Both mechanisms of enhancing the galactic annihilation have been widely discussed (see *e.g.* [81]) in an attempt to link some cosmic-ray anomalies—such as an elevated positron fraction $e^+/(e^- + e^+)$ observed by the PAMELA satellite experiment [84]—to dark matter annihilation. For example, an attractive $-\alpha'/r$ potential in the WIMP sector leads to a significant enhancement of annihilation at low velocities via a well-known Sommerfeld factor $\sigma v \sim (\pi\alpha'/v)[1 - \exp(-\pi\alpha'/v)]^{-1}$; when $v \lesssim \pi\alpha'$, $S(v) \simeq \pi\alpha'/v$. This enhancement, in turn, generates a $\sim T^{-1/2}$ scaling of $\langle S(v) \rangle_T$ in (30) when WIMPs are still in kinetic

equilibrium with the plasma. Once the WIMPs' interactions with the thermalized plasma species have ceased, $\langle S(v) \rangle_T$ falls even more rapidly as $\sim T^{-1}$. Therefore, the fraction of WIMPs annihilated in a Hubble time scales with photon temperature as follows:

$$\text{Sommerfeld enhancement:} \quad \begin{cases} f_X(T) \sim T^{1/2} & \text{kinetic equilibrium} \\ f_X(T) \sim \text{const} & \text{kinetically decoupled} \end{cases}$$

Similarly, the presence of narrow resonances just above the XX annihilation threshold may drastically boost the annihilation at low energies. For a narrow resonance at some energy E_R above the di-WIMP threshold the pattern of energy injection has a sharp cutoff:

$$\text{Resonant enhancement:} \quad \begin{cases} f_X(T) \sim \exp(-E_R/T) & \text{kinetic equilibrium} \\ f_X(T) \sim \exp(-E_R T_{kd}/T^2) & \text{kinetically decoupled} \end{cases}$$

where T_{kd} is the temperature of WIMP kinetic decoupling. Notably, the last pattern (resonant annihilation, kinetically decoupled WIMPs) has the same time dependence as the energy injection as particle decays, $\exp(-t/\tau_X)$, on account of the $t \sim 1/T^2$ relation. If the annihilation cross sections $\langle \sigma v \rangle(t_{\text{BBN}})$ are enhanced by some large factor, $\sim \mathcal{O}(10^3)$, relative to the fiducial WIMP rate $(\sigma v)_0$, then WIMP physics can have a significant impact on the primordial abundance of ${}^6\text{Li}$. However, a large class of models that predict the WIMP-enhancement of the PAMELA positron signal produce light particles (photons, electrons, light mesons) via annihilation, which has a much weaker effect on ${}^6\text{Li}$.

A case of independent interest is the decay of a WIMP-like state with a stable non-SM particle in the final state. The initial abundance of so-called ‘‘parent’’ WIMPs is given by its annihilation at the freeze-out, whereas their decays may source the dark matter energy density. If the amount of energy released in such decays is on the order of the parent WIMP mass, then in such a scenario an amount of energy comparable to the dark matter energy density could be released into the primordial plasma. If so, BBN with energy injection sets a rather strict constraint: The lifetime of the parent particle must be less than $\sim 10^7$ s if the decays are fully electromagnetic and shorter than 10^4 s if there is a significant hadronic component among the decays products. In the next section we explain that the sensitivity to the lifetime of such parent WIMP particles can be even stronger if they carry negative electric charge.

4 CATALYZED BBN

In this section we discuss changes to BBN in a scenario where particles from a new physics sector *participate* in thermal nuclear reactions before decaying. Such an unusual situation may arise if the particles are charged under the electromagnetic or strong group of the SM [85]. The idea of particle physics catalysis of nuclear reactions dates from the 1950s, when muon-catalyzed fusion became a subject of active theoretical and experimental research in nuclear physics. More recently, interest in the possibility of nuclear catalysis by

hypothetical negatively charged particles that live long enough to participate in nuclear reactions at the time of BBN has intensified [85, 86, 87, 76, 88, 89, 90, 91, 92, 93, 94, 53, 95] (see also Ref. [96, 97, 98] for earlier work on the subject). The essence of the idea is very simple: A negatively charged massive particle, which we term X^- , gets into a bound state with the nucleus of mass m_N and charge Z , forming a large compound nucleus with charge $Z - 1$, mass $M_X + m_N$, and binding energy in the $\mathcal{O}(0.1 - 1)$ MeV range. Once the bound state is formed, the Coulomb barrier is reduced, signaling higher “reactivity” between the compound nucleus and other nuclei. Even more importantly, new reaction channels may open up and avoid SBBN-suppressed production mechanisms [85], *e.g.* Eq. (17), thus clearing the path to the synthesis of very rare isotopes such as ${}^6\text{Li}$ and ${}^9\text{Be}$.

Interest in catalyzed BBN (CBBN) is partly motivated by a possible connection to dark matter. Even though dark matter should not be charged, it is possible that it comes with a relatively long-lived charged counterpart. An example of this kind is weak-scale supersymmetry (SUSY), where the lightest supersymmetric particle (LSP) being the gravitino and the next-to-LSP (NLSP) a charged slepton. In that case the decay of the NLSP is greatly delayed by the smallness of the gravitino-lepton-slepton coupling $\sim M_{\text{Pl}}^{-1}$. Another example in the same vein is a nearly degenerate stau-neutralino system, in which case the longevity of the charged stau against the decay to the dark matter neutralino is ensured as long as the mass splitting of the stau-neutralino system is below 100 MeV [99]. In these two examples, both, the gravitino and neutralino represent viable dark matter candidates. A very important aspect of CBBN is that the abundance of charged particles before they begin to decay is given by their annihilation rate at freeze-out. In most models these particles’ abundance is easy to calculate. If no special mechanisms are introduced to boost the annihilation rate, then the abundance of charged particles per nucleon is not small [typical range of $Y_X = n_X/n_b \sim (0.001 - 0.1)m_X/\text{TeV}$]. Moreover, the charged states accompanying dark matter are often required in order to facilitate the WIMP annihilation process which results in a cosmologically acceptable dark matter abundance—a phenomenon known as co-annihilation.

4.1 Catalysis by stable charged particles.

In this section we describe BBN catalysis by use of negatively charged heavy relics X^- ; we do not attempt to place this phenomenon in a specific particle physics model framework, and we *ignore* the effects of energy injection due to the X^- decay. We describe an elementary particle, so typical collider bounds would require $m_{X^-} \gtrsim 100$ GeV.

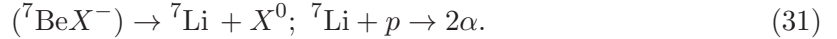
4.1.1 PROPERTIES OF THE BOUND STATES. For light nuclei that participate in BBN, we can assume that the reduced mass of the nucleus- X^- system is well approximated by the nuclear mass, so that the binding energy is given by $Z^2\alpha^2 m_A/2$ when the Bohr orbit is larger than the nuclear radius. However, this is a poor approximation for all nuclei heavier than $A = 4$, and the effect of the finite nuclear charge radius must be taken into account. In Table 1 we give the binding energies and the recombination temperature for each bound state. The

bound state	a_0 [fm]	$ E_b $ [keV]	T_0 [keV]
(pX^-)	29	25	0.6
$({}^4\text{He}X^-)$	3.63	346	8.2
$({}^7\text{Be}X^-)$	1.03	1350	32
$({}^8\text{Be}X^-)$	0.91	1430	34

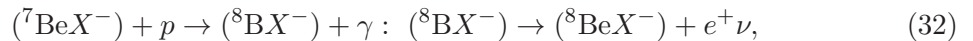
Table 1: Properties of the bound states: Bohr radius $a_0 = 1/(Z\alpha m_N)$, binding energies E_b calculated for realistic charge radii, and “photo-dissociation decoupling” temperatures T_0 .

recombination temperature is the temperature at which the photodissociation rate of bound states becomes smaller than the Hubble expansion rate. Below these temperatures, bound states are practically stable. The most important benchmark temperatures for CBBN are $T \sim 30$, 8, and 0.5 keV for the respective bound states $({}^7\text{Be}X^-)$, $({}^4\text{He}X^-)$, and (pX^-) when they can be formed without efficient suppression by the photodissociation processes. Importantly, these properties of the bound states are generic to any CBBN realization when X^- does not participate in strong interactions; in other words, they are determined entirely by the charge of X^- and electromagnetic properties of the nuclei and therefore are applicable to SUSY and non-SUSY models alike. Also, the $({}^8\text{Be}X^-)$ compound nucleus is stable, which may open the path to synthesis of $A > 8$ elements in CBBN.

4.1.2 CATALYSIS AT 30 KEV: SUPPRESSION OF ${}^7\text{Be}$. While the Universe cools to temperatures of 30 keV, the abundances of D, ${}^3\text{He}$, ${}^4\text{He}$, ${}^7\text{Be}$ and ${}^7\text{Li}$ are already close to their freeze-out values, although several nuclear processes remain faster than the Hubble rate. At such temperatures, a negatively charged relic can get into bound states with ${}^7\text{Be}$ and form a $({}^7\text{Be}X^-)$ composite object through the photo-recombination process. Once a composite object is formed, new destruction mechanisms for ${}^7\text{Be}$ appear. For models with weak currents connecting nearly mass-degenerate X^- and X^0 states, a very fast internal conversion followed by the p -destruction of ${}^7\text{Li}$ becomes possible:



Alternatively, ${}^7\text{Li}$ can be destroyed via recombination with X^- and subsequent conversion to unstable ${}^7\text{He}$ [90]. When a $X^- \rightarrow X^0$ weak transition is not allowed, the destruction of ${}^7\text{Be}$ can be achieved via the following chain:



which is greatly enhanced by atomic resonances in the $({}^7\text{Be}X^-)$ system [89].

The rates for both mechanisms may be faster than the Hubble rate and may therefore lead to a sizable suppression of ${}^7\text{Be}$ abundance if $({}^7\text{Be}X^-)$ bound states are forming efficiently. In other words, $({}^7\text{Be}X^-)$ serves as a bottleneck for the CBBN depletion of ${}^7\text{Be}$. The recombination rate per ${}^7\text{Be}$ nucleus leading to $({}^7\text{Be}X^-)$ is given by the product of

the recombination cross section and the concentration of X^- -particles. It is easy to show that for $Y_X \lesssim 0.01$ the recombination rate is too slow to lead to a significant depletion of ${}^7\text{Be}$. Detailed calculations of the recombination rate and numerical analyses of CBBN at 30 keV [89,94] find that a suppression of ${}^7\text{Be}$ by a factor of two is possible for (a) $Y_X \geq 0.1$ if the mechanism in Eq. (32) alone is operative, and (b) for $Y_X \geq 0.02$, if the internal conversion of Eq. (31) is allowed. Even if $Y_X \sim \mathcal{O}(0.1 - 1)$, X^0 could still be compatible with dark matter as long as m_{X^0} is suppressed relative to m_{X^-} .

4.1.3 CATALYSIS AT 8 KEV: ENHANCEMENT OF ${}^6\text{Li}$ AND ${}^9\text{Be}$. As the Universe continues to cool below 10 keV, the efficient formation of $({}^4\text{He}X^-)$ bound states becomes possible. If we make the reasonable assumption that $Y_X \lesssim Y_{\text{He}}$ then the rate of formation of bound states per X^- particle is given by the recombination cross section and the concentration of the helium nuclei. A numerical analysis of recombination reveals that at $T \simeq 5$ keV approximately 50% of the available X^- particles are in bound states with ${}^4\text{He}$ [85].

As soon as $({}^4\text{He}X^-)$ is formed, new reaction channels open up. In particular, a photonless thermal production of ${}^6\text{Li}$ becomes possible



This rate exceeds the SBBN production rate by approximately six orders of magnitude. The production of ${}^9\text{Be}$ may also be catalyzed, possibly by many orders of magnitude relative to the SBBN values, with the following thermal nuclear chain [93]:



Both reactions at these energies are dominated by resonant contributions, although the efficiency of the second process in (34) is not fully understood. (A recent calculation [95] places the resonance found in the $({}^9\text{Be}X^-)$ system [93] below the threshold. However, because this is a reaction with a neutral particle, even the sub-threshold resonance may give a strong enhancement of the neutron capture.)

Current estimates and calculations of the CBBN rates are used to determine the generic constraints on the lifetimes and abundances of charged particles. The essence of these limits is depicted in Figures 8 and 9, which shows that for typical X^- abundances the lifetime of the charged particles would have to be limited by a few thousand seconds (unless a special mechanism for suppressing Y_X is found, as in *e.g.* [100,101]). This is the most important fact to be learned from the catalysis of BBN by charged particles. Although to lowest order non-thermal BBN is sensitive to the energy density of decaying particles, the CBBN processes are controlled by the number density of X^- , which underscores the complementary character of these constraints. In some models, in which both catalysis and non-equilibrium nucleosynthesis occur, catalysis dominates the non-thermal production of ${}^6\text{Li}$ for all particles with hadronic branching ratio $B_h \lesssim 10^{-2}$ [92], whereas ${}^7\text{Li}$ destruction is usually dominated by neutron injection effects unless $B_h \lesssim 10^{-4}$.

4.1.4 CATALYSIS BELOW 1 KEV? Finally we comment on the possibility of (pX^-) catalysis of nuclear reactions, discussed in Refs. [97,91]. Although it is conceivable that the

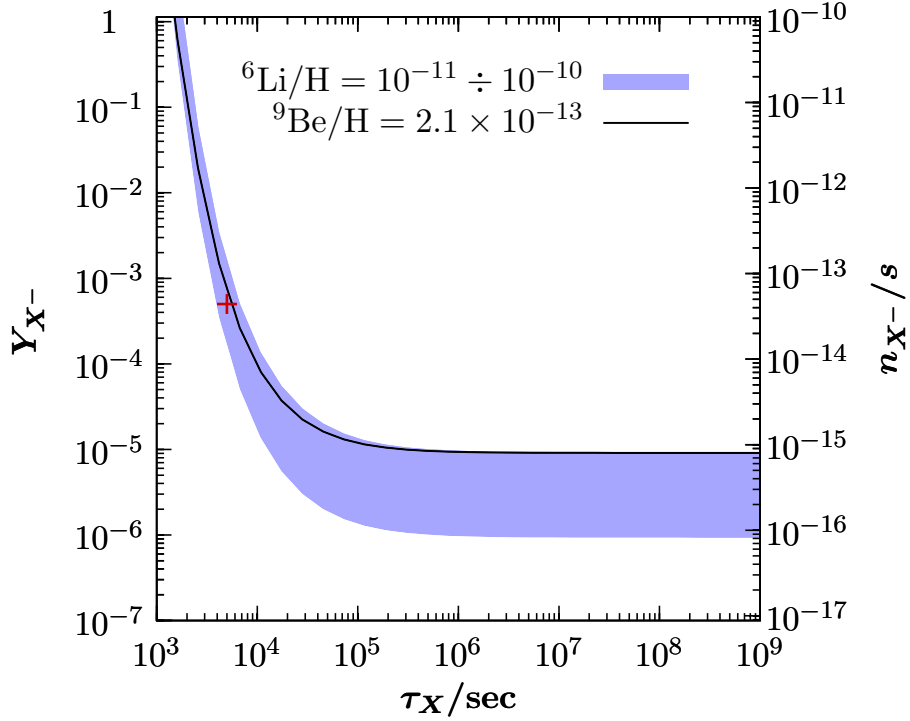


Figure 8: CBBN constraints on the abundance versus lifetime of X^- . The red cross corresponds to a point in the parameter space; the temporal development of ${}^6\text{Li}$ and ${}^9\text{Be}$ for this point is shown in Figure 9 [53].

absence of the Coulomb barrier for this compound nucleus may lead to significant changes of SBBN/CBBN predictions, in practice (pX^-)-related mechanisms are of only secondary importance in most cases. The large radius and shallow binding of this system leads to a fast charge-exchange reaction on helium: $(pX^-) + {}^4\text{He} \rightarrow ({}^4\text{He}X^-) + p$. This reaction reduces the abundance of (pX^-) below 10^{-6} relative to hydrogen, as long as $Y_{X^-} \lesssim Y_{4\text{He}}$, making further reactions inconsequential for any observable element [53]. In the less likely case in which $Y_{X^-} \gtrsim Y_{4\text{He}}$, significant late-time processing due to (pX^-) bound states may still occur. Nevertheless, such late-time BBN typically leads to observationally unacceptable final BBN yields.

Unlike in the SBBN case and even in non-equilibrium nucleosynthesis that utilizes mostly measured nuclear reaction rates, CBBN rates cannot be measured in the laboratory; significant nuclear theory input for the calculation of the reaction rates is required. However, because the X^- participates only in electromagnetic interactions, such calculations are feasible, and dedicated nuclear theory studies [88, 95] for certain important CBBN processes [such as those of Eqs. (32) and (33)] have already been performed.

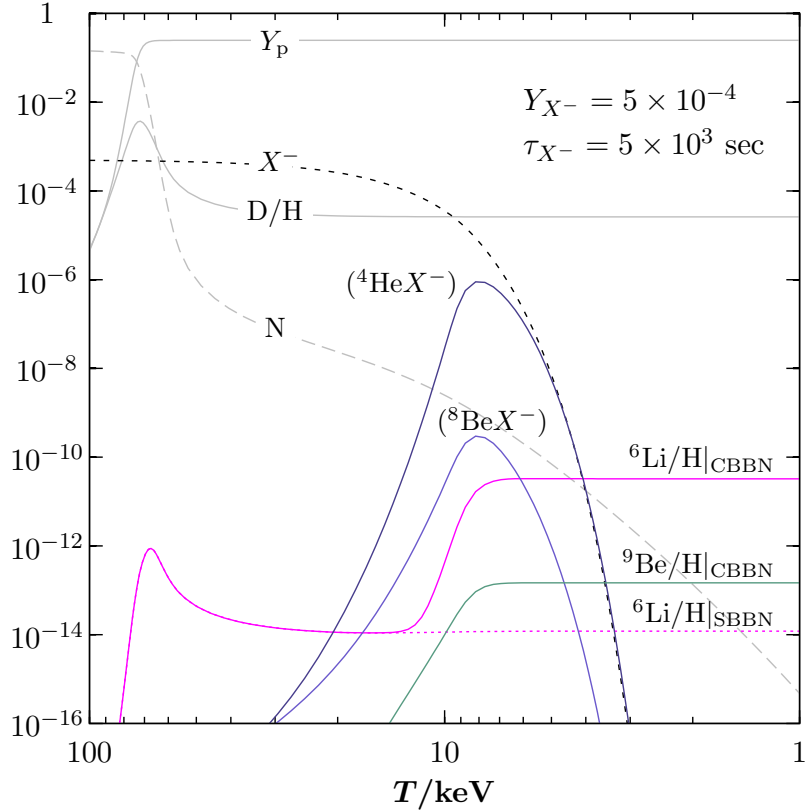


Figure 9: The temperature evolution of the bound state abundances (${}^4\text{He}X^-$) and (${}^8\text{Be}X^-$), as well as the synthesis of ${}^6\text{Li}$ and ${}^9\text{Be}$ at $T \sim 8$ keV. The initial abundance of negatively charged particles is $Y_{X^-} = 5 \times 10^{-4}$ and the lifetime is 5000 s.

4.2 Catalysis by strongly interacting relics

Catalysis by strongly interacting relics, X_s , is another generic possibility that has recently been addressed [102,103]. The main difficulty of this scenario lies in determining the properties of the composite nuclei that contain X_s . For some types of X_s , some progress can be made. Specifically, if X_s represents an isospin doublet similar to (n, p) , one could draw some conclusions about the binding energies with nucleons by utilizing our extensive theoretical knowledge of two-nucleon systems. For example, a heavy scalar quark (or squark), would attract one light quark and become a spin-1/2 “mesino” with similar interaction properties as normal nucleons. In other examples involving a particle in the adjoint representation, such as a gluino, it is almost impossible at this point to determine whether it would bind to a single nucleon and, if so, with what energy. Regardless of the type of strongly interacting relic, the relic’s abundance is expected to be suppressed by more than five orders of magnitude compared with X^- due to a very efficient annihilation channel following hadronization [104].

Detailed investigations of mesino-nucleon bound systems [103] offer insight into X_s -catalyzed BBN. By making fairly generous assumptions about the uncertainties in the

interaction strength, the binding energy of the mesino-nucleon system would typically be between 5 and 40 MeV, which is much larger than the deuteron binding energy E_d . A tighter bound nucleon-mesino system is expected, because the shallow binding of the deuteron is to some extent “accidental”, and because going from a nucleon-nucleon system to a nucleon-mesino decreases the kinetic energy and results in a stronger binding. The main cosmological consequence of a tightly-bound mesino-nucleon system is the formation of such bound states long *before* the end of the SBBN deuterium bottleneck, and, hence, at times when neutrons are abundant. For example, a ~ 20 MeV binding would correspond to a new bottleneck at $T \sim 1$ MeV, thereby opening up an interesting new possibility for nucleosynthesis in the neutron-rich environment *around* each X_s particle. Unfortunately, a detailed study of such a nucleosynthetic path is currently beyond theoretical capabilities, mostly due to the rather uncertain spectrum of light mesino-containing nuclei. While certain claims were made that nucleosynthesis proceeds to form the $A \geq 6$ elements [102], it appears equally plausible that nucleosynthesis around strongly interacting particles stops at a “compound helium”—a bound state consisting of a mesino particle and three nucleons. Nucleosynthesis of heavier elements around a mesino may be inhibited by (p, α) reactions, as well as by an expected weak binding in a system containing five particles (one mesino and four nucleons) [103]. It is fair to say that much more theoretical work will be required before we fully understand the primordial catalysis caused by strongly-interacting particles.

5 CONCLUSIONS

Big Bang Nucleosynthesis, a very short period in the history of the Universe, is an important reference point going back to cosmological times of a few seconds. In this review we have shown how new physics can modify the synthesis of light elements and therefore be probed by contrasting the observations of helium and deuterium (as well as lithium, beryllium, and boron) with the BBN predictions. All three generic methods—modifications to the timing of main BBN events via extra degrees of freedom or space-time dependent couplings and mass scales, non-equilibrium nucleosynthesis triggered by energy injection via the annihilation or decay of heavy particles, and particle catalysis of BBN reactions—are very important to many extensions of the Standard Model. In some models, the sensitivity of BBN to new physics is exceptional and indeed exceeds all other direct and indirect probes. A representative example is the non-trivial limit on the lifetime of a metastable charged particle (*e.g.* a stau decaying to a gravitino) that follows from the considerations of the ${}^6\text{Li}$ abundance, a limit that currently cannot be constrained other than in BBN.

The amount of lithium predicted by SBBN is of the same order of magnitude as the value indicated by the Spite plateau. However, a detailed comparison with the standard cosmology and particle physics input shows that SBBN over-predicts the abundance of ${}^7\text{Li}$ by a factor of three to five. This discrepancy has become more concrete, given that the baryon-to-photon ratio and the main SBBN reactions determining ${}^7\text{Li}$ abundance are known to an accuracy of better than 10%. We have suggested possible solutions to the

problem that may reside in subtle astrophysical effects, or in new cosmological and/or particle physics ingredients. Here we summarize these (and some additional) options

- The most economical solution to the lithium discrepancy would be an astrophysical mechanism that depletes lithium from the photic zone in the atmospheres of population II stars. Several ideas as to the nature of this mechanism have been proposed in the literature, and hints at traces of such depletion in the scatter of points along the Spite plateau have been found [44]. Although some amount of depletion is certainly possible, it is premature to concede that it can account for the discrepancy of a factor of approximately three. Clearly that this issue remains one of the most important astrophysical issues in the cosmology of the early Universe.
- Nuclear physics is unlikely to be responsible for the solution to the lithium problem, as all main reactions participating in creation and destruction of lithium are well known. Perhaps the last subject worth of detailed investigation is a possible resonant enhancement of the ${}^7\text{Be}+\text{D}$ reaction [46], which could contribute to the depletion of ${}^7\text{Be}$, albeit at the very end of the most optimistic range for the parameters of such a resonance. This issue can be directly clarified through experiments.
- Given that lithium is observed in the Milky Way, whereas the measurements of deuterium and especially η_b are global, one may speculate that baryons and possibly dark matter are distributed non-uniformly and that the 30-50% downward fluctuation of η_b at the local patch of the Universe leads to a local value of lithium that is close to the Spite plateau value (see *e.g.* [105] for a recent discussion). Of course, the variations in baryon number by a factor of a few, if persistent at all scales, would create very strong isocurvature-type features in the CMB polarization maps. However, it is also possible that models with anticorrelated baryon-dark matter fluctuations with a very blue perturbation spectrum may survive all observational constraints.
- Particle physics models with unstable or annihilating particles may have an important effect on the lithium abundance. Although the photo-disintegration of lithium by a factor of three is difficult to reconcile with the deuterium abundance and/or the ${}^3\text{He}/\text{D}$ ratio (unless the mass of a decaying particle is carefully chosen), the energy injection with some yield of nucleons in the final state may fare much better. Indeed, the injection of neutrons (regardless of the details of the particle physics mechanism) *before* the freeze-out of ${}^7\text{Li}(p, \alpha)\alpha$ reaction can reduce the ${}^7\text{Be}$ and therefore ${}^7\text{Li}$ abundance. A necessary consequence of this scenario is a somewhat elevated D/H abundance, and probably elevated concentrations of other rare isotopes of lithium (and possibly beryllium and boron).
- The catalytic suppression of ${}^7\text{Li}$ by negatively charged particles relies on the fact that $({}^7\text{Be}X^-)$ is the deepest bound state among all X^- -bound nuclei which can form at temperatures of approximately 30 keV. The most efficient suppression of ${}^7\text{Be}$ happens in models allowing for weak transitions to ${}^7\text{Li}$ at these temperatures. The need for a

large number of X^- at 30 keV also implies the presence of X^- at $T \sim 10$ keV, which would lead to the catalyzed synthesis of ${}^6\text{Li}$ and ${}^9\text{Be}$.

- The last and perhaps most exotic option is the possibility of coupling constants and mass scales changing over time. Indeed, a $\sim 5\%$ change in the deuterium binding energy can create a very strong downward shift of the ${}^7\text{Li}$ abundance, while remaining consistent with helium and deuterium abundances.

We do not yet know how to resolve the lithium problem; only continuing progress in particle physics, cosmology, and astrophysics will help to clarify this intriguing discrepancy.

Finally, we discuss some anticipated future developments that are not necessarily directly related to BBN but rather are related to questions discussed in our review.

- CMB physics will continue to deliver very important results. Of particular interest to this review is the increased sensitivity on small angular scales (high- l multipoles) where the effects of extra “dark radiation” states or certain types of isocurvature fluctuations are the most pronounced. Future data from the Planck satellite experiment will allow us to probe the dark radiation energy density with an accuracy of $\Delta N_{\nu,\text{eff}} \sim 0.5$ or better; results thus obtained will thereby provide an independent check of the constraints resulting from ${}^4\text{He}$ abundances.
- The Large Hadron Collider is expected to deliver its first physics results in the near future. The TeV energy frontier will be effectively probed, which may lead to the discovery of stable or massive metastable particles. If such particles were neutral, their signature would constitute “missing energy”, which is difficult but not impossible to disentangle from SM processes. However, if a metastable particle were charged a under strong or electromagnetic gauge group, the signatures would be much more spectacular, with long charged tracks that would allow us to identify the mass of such objects. If charged metastable states are discovered at the LHC, the theories of non-equilibrium and catalyzed nucleosynthesis would be further reinforced.
- A massive expansion of the dark matter search program, both in space and in underground laboratories, may point to the existence of WIMPs in the near future. If WIMPs turn out to be relatively light (in the 10-50 GeV window), then the energy injection in the early universe could lead to altered ${}^7\text{Li}$ and ${}^6\text{Li}$ abundances. Heavier WIMPs with enhanced annihilation cross sections devised to fit the PAMELA positron anomaly [84] may also lead to changes in lithium abundances, and therefore any future development that supports or disfavors the WIMP interpretation of the PAMELA anomaly is of interest for the BBN predictions.
- Finally, further theoretical progress in non-SBBN scenarios is expected. Given the doubtful status of ${}^6\text{Li}$ observations and its extreme fragility, it is highly desirable to perform calculations of beryllium and boron abundances generated in BBN scenarios with energy injection. Doing so may place further constraints on annihilating/decaying WIMP scenarios. Additionally, more detailed calculations of some

CBBN rates with a proper many-body nuclear physics input are needed.

LITERATURE CITED

1. Alpher RA, Follin JW, Herman RC, *Phys.Rev* 92:1347 (1953).
2. Dunkley J, et al., *Astrophys. J. Suppl.* 180:306 (2009), 0803.0586.
3. Alpher RA, Bethe H, Gamow G, *Phys.Rev.Lett* 73:803 (1948).
4. Alpher R, Herman RC, *Rev. Mod. Phys.* 22:153 (1950).
5. Hayashi C, *Progr. Theor. Phys.* 5:224 (1950).
6. Malaney RA, Mathews GJ, *Phys. Rept.* 229:145 (1993).
7. Sarkar S, *Rept. Prog. Phys.* 59:1493 (1996), hep-ph/9602260.
8. Iocco F, Mangano G, Miele G, Pisanti O, Serpico PD, *Phys. Rept.* 472:1 (2009), 0809.0631.
9. Steigman G, *Ann. Rev. Nucl. Part. Sci.* 57:463 (2007), 0712.1100.
10. Jedamzik K, Pospelov M, *New J. Phys.* 11:105028 (2009), 0906.2087.
11. Dolgov AD, Fukugita M, *Phys. Rev. D*46:5378 (1992).
12. Wagoner RV, Fowler WA, Hoyle F, *Astrophys. J.* 148:3 (1967).
13. Mukhanov VF, *Int. J. Theor. Phys.* 43:669 (2004), astro-ph/0303073.
14. Kawano L, FERMILAB-PUB-92-004-A.
15. Audi G, Wapstra AH, Thibault C, *Nucl. Phys.* A729:337 (2002).
16. Mohr PJ, Taylor BN, *Rev. Mod. Phys.* 77:1 (2005).
17. Descouvemont P, Adahchour A, Angulo C, Coc A, Vangioni-Flam E, *Atomic Data and Nuclear Data Tables* 88:203 (2004), arXiv:astro-ph/0407101.
18. Ando S, Cyburt RH, Hong SW, Hyun CH, *Phys. Rev. C*74:025809 (2006), nucl-th/0511074.
19. Cyburt RH, Davids B, *Phys. Rev. C*78:064614 (2008), 0809.3240.
20. Lopez RE, Turner MS, *Phys. Rev. D*59:103502 (1999), astro-ph/9807279.
21. Wilkinson DH, *Nucl. Phys.* A377:474 (1982).
22. Cyburt RH, Fields BD, Olive KA, *JCAP* 0811:012 (2008), 0808.2818.
23. Peimbert M, Luridiana V, Peimbert A, *Astrophys. J.* 666:636 (2007), astro-ph/0701580.
24. Izotov YI, Thuan TX, Stasinska G, *Astrophys. J.* 662:15 (2007), astro-ph/0702072.
25. Olive KA, Skillman ED, *Astrophys. J.* 617:29 (2004), astro-ph/0405588.
26. Fukugita M, Kawasaki M, *Astrophys. J.* 646:691 (2006).
27. Burles S, Tytler D, *Astrophys. J.* 499:699 (1998), astro-ph/9712108.
28. Levshakov SA, Dessauges-Zavadsky M, D'Odorico S, Molaro P, *Astrophys. J.* 565:696 (2002), astro-ph/0105529.
29. Crighton NHM, Webb JK, Ortiz-Gill A, Fernandez-Soto A, *Mon. Not. Roy. Astron. Soc.* 355:1042 (2004), astro-ph/0403512.

30. O'Meara JM, et al., *Astrophys. J.* 649:L61 (2006), astro-ph/0608302.
31. Pettini M, Zych BJ, Murphy MT, Lewis A, Steidel CC, *MNRAS* 391:1499 (2008), 0805.0594.
32. Linsky JL, et al., *Astrophys. J.* 647:1106 (2006), astro-ph/0608308.
33. Prodanovic T, Steigman G, Fields BD, (2009), 0910.4961.
34. Sigl G, Jedamzik K, Schramm DN, Berezhinsky VS, *Phys. Rev. D* 52:6682 (1995), astro-ph/9503094.
35. Geiss J, Gloeckler G, *Space Science Reviews* 130:5 (2007).
36. Nara Singh BS, Hass M, Nir-El Y, Haquin G, *Phys. Rev. Lett.* 93:262503 (2004), nucl-ex/0407017.
37. Gyurky G, et al., *Phys. Rev. C* 75:035805 (2007), nucl-ex/0702003.
38. Brown TAD, et al., *Phys. Rev. C* 76:055801 (2007), 0710.1279.
39. Melendez J, Casagrande L, Ramirez I, Asplund M, Schuster WJ, (2009), 0912.2949.
40. Aoki W, et al., *Astrophys. J.* 698:1803 (2009), 0904.1448.
41. Ryan SG, Norris JE, Beers TC, *Astrophys. J.* 523:654 (1999), astro-ph/9903059.
42. Bonifacio P, Pasquini L, Spite F, Bragaglia A, Carretta E, et al., *A&A* 390:91 (2002), arXiv:astro-ph/0204332.
43. Pasquini L, Molaro P, *Astron. Astrophys.* 322:109 (1997), astro-ph/9612158.
44. Asplund M, Lambert DL, Nissen PE, Primas F, Smith VV, *Astrophys. J.* 644:229 (2006), astro-ph/0510636.
45. Coc A, Vangioni-Flam E, Descouvemont P, Adahchour A, Angulo C, *Astrophys. J.* 600:544 (2004), astro-ph/0309480.
46. Cyburt RH, Pospelov M, (2009), 0906.4373.
47. Angulo C, et al., *Astrophys. J.* 630:L105 (2005), astro-ph/0508454.
48. Richard O, Michaud G, Richer J, *Astrophys. J.* 619:538 (2005), astro-ph/0409672.
49. Korn A, et al., *Nature* 442:657 (2006), astro-ph/0608201.
50. Primas F, Asplund M, Nissen PE, Hill V, *A&A* 364:L42 (2000), arXiv:astro-ph/0009482.
51. Boesgaard AM, Novicki MC, *Astrophys. J.* 641:1122 (2006), astro-ph/0512317.
52. Fields BD, Olive KA, Vangioni-Flam E, *Astrophys. J.* 623:1083 (2005), astro-ph/0411728.
53. Pospelov M, Pradler J, Steffen FD, *JCAP* 0811:020 (2008), 0807.4287.
54. Prantzos N, *A&A* 448:665 (2006), arXiv:astro-ph/0510122.
55. Cayrel R, Steffen M, Chand H, Bonifacio P, Spite M, et al., *A&A* 473:L37 (2007), 0708.3819.
56. Ratra B, Peebles PJE, *Phys. Rev. D* 37:3406 (1988).
57. Wetterich C, *Nucl. Phys. B* 302:668 (1988).
58. Flambaum VV, Shuryak EV, *Phys. Rev. D* 65:103503 (2002), hep-ph/0201303.

59. Flambaum VV, Wiringa RB, Phys. Rev. C76:054002 (2007), 0709.0077.
60. Nollett KM, Lopez RE, Phys. Rev. D66:063507 (2002), astro-ph/0204325.
61. Dmitriev VF, Flambaum VV, Webb JK, Phys. Rev. D69:063506 (2004), astro-ph/0310892.
62. Coc A, Nunes NJ, Olive KA, Uzan JP, Vangioni E, Phys. Rev. D76:023511 (2007), astro-ph/0610733.
63. Dent T, Stern S, Wetterich C, Phys. Rev. D76:063513 (2007), 0705.0696.
64. Voronchev VT, Nakao Y, Nakamura M, JCAP 0805:010 (2008).
65. Ellis JR, Nanopoulos DV, Sarkar S, Nucl. Phys. B259:175 (1985).
66. Levitan YL, Sobol IM, Khlopov MY, Chechetkin VM, Sov. J. Nucl. Phys. 47:109 (1988).
67. Dimopoulos S, Esmailzadeh R, Hall LJ, Starkman GD, Astrophys. J. 330:545 (1988).
68. Reno MH, Seckel D, Phys. Rev. D37:3441 (1988).
69. Dimopoulos S, Esmailzadeh R, Hall LJ, Starkman GD, Nucl. Phys. B311:699 (1989).
70. Ellis JR, Gelmini GB, Lopez JL, Nanopoulos DV, Sarkar S, Nucl. Phys. B373:399 (1992).
71. Khlopov MY, Levitan YL, Sedelnikov EV, Sobol IM, Phys. Atom. Nucl. 57:1393 (1994).
72. Kawasaki M, Moroi T, Astrophys. J. 452:506 (1995), astro-ph/9412055.
73. Jedamzik K, Phys. Rev. D70:063524 (2004), astro-ph/0402344.
74. Kawasaki M, Kohri K, Moroi T, Phys. Lett. B625:7 (2005), astro-ph/0402490.
75. Kawasaki M, Kohri K, Moroi T, Phys.Rev.D 71:083502 (2005), astro-ph/0408426.
76. Cyburt RH, Ellis JR, Fields BD, Olive KA, Spanos VC, JCAP 0611:014 (2006), astro-ph/0608562.
77. Cyburt RH, et al., JCAP 0910:021 (2009), 0907.5003.
78. Protheroe RJ, Stanev T, Berezhinsky VS, Phys. Rev. D51:4134 (1995), astro-ph/9409004.
79. Cyburt RH, Ellis JR, Fields BD, Olive KA, Phys. Rev. D67:103521 (2003), astro-ph/0211258.
80. Ellis JR, Olive KA, Vangioni E, Phys. Lett. B619:30 (2005), astro-ph/0503023.
81. Pospelov M, Ritz A, Phys. Lett. B671:391 (2009), 0810.1502.
82. Pospelov M, Pradler J, work in progress. (2010).
83. Jedamzik K, Phys. Rev. D70:083510 (2004), astro-ph/0405583.
84. PAMELA, Adriani O, et al., Nature 458:607 (2009), 0810.4995.
85. Pospelov M, Phys. Rev. Lett. 98:231301 (2007), hep-ph/0605215.
86. Kohri K, Takayama F, Phys. Rev. D76:063507 (2007), hep-ph/0605243.
87. Kaplinghat M, Rajaraman A, Phys. Rev. D74:103004 (2006), astro-ph/0606209.
88. Hamaguchi K, Hatsuda T, Kamimura M, Kino Y, Yanagida TT, Phys. Lett. B650:268

- (2007), hep-ph/0702274.
89. Bird C, Koopmans K, Pospelov M, Phys. Rev. D78:083010 (2008), hep-ph/0703096.
 90. Jittoh T, et al., Phys. Rev. D76:125023 (2007), 0704.2914.
 91. Jedamzik K, Phys. Rev. D77:063524 (2008), 0707.2070.
 92. Jedamzik K, JCAP 0803:008 (2008), 0710.5153.
 93. Pospelov M, (2007), 0712.0647.
 94. Kusakabe M, Kajino T, Boyd RN, Yoshida T, Mathews GJ, ApJ680:846 (2008), 0711.3858.
 95. Kamimura M, Kino Y, Hiyama E, Progress of Theoretical Physics 121:1059 (2009), 0809.4772.
 96. De Rujula A, Glashow SL, Sarid U, Nucl. Phys. B333:173 (1990).
 97. Dimopoulos S, Eichler D, Esmailzadeh R, Starkman GD, Phys. Rev. D41:2388 (1990).
 98. Rafelski J, Sawicki M, Gajda M, Harley D, Phys. Rev. A44:4345 (1991).
 99. Jittoh T, Sato J, Shimomura T, Yamanaka M, Phys. Rev. D73:055009 (2006), hep-ph/0512197.
 100. Ratz M, Schmidt-Hoberg K, Winkler MW, JCAP 0810:026 (2008), 0808.0829.
 101. Pradler J, Steffen FD, Nucl. Phys. B809:318 (2009), 0808.2462.
 102. Kusakabe M, Kajino T, Yoshida T, Mathews GJ, Phys. Rev. D80:103501 (2009), 0906.3516.
 103. Sharman J, M.Sc. thesis, University of Victoria (2010).
 104. Kang J, Luty MA, Nasri S, JHEP 09:086 (2008), hep-ph/0611322.
 105. Holder GP, Nollett KM, van Engelen A, (2009), 0907.3919.